https://doi.org/10.15407/ufm.27.03.566

**G.A. KONONENKO [1–3,*], P. RAMASAMY [4,5,**], S.V. ADJAMSKY [1,6,***], J. ECKERT [4,5,****], R.V. PODOLSKYI [1,2,7,*****], O.A. PODOLSKA [2], and S.I. BADUK [1,7]**

[1] LLC Additive Laser Technologies of Ukraine',
105, Nebesnoi Sotni Ave., UA-65104 Odesa, Ukraine
[2] Iron and Steel Institute of Z.I. Nekrasov of the N.A.S. of Ukraine,
1, Academician Starodubov Sq., UA-49107 Dnipro, Ukraine
[3] National Technical University of Ukraine 'Dnipro Polytechnic',
19, Dmytro Yavornytskyi Ave., UA-49005 Dnipro, Ukraine
[4] Erich Schmid Institute of Materials Science of the Austrian Academy of Sciences,
12, Jahnstraße, A-8700 Leoben, Austria
[5] Department of Materials Science, Chair of Materials Physics, Montanuniversität Leoben, Jahnstraße 12, A-8700 Leoben, Austria
[6] Institute of Transport Systems and Technologies of the N.A.S. of Ukraine,
5, Pisarzhevskoho Str., UA-49000 Dnipro, Ukraine
[7] Institute of Applied Control Systems of the N.A.S. of Ukraine,
40, Academician Hlushkov Ave., UA-03187 Kyiv, Ukraine

* perlit@ua.fm, ** parthiban.ramasamy@oeaw.ac.at, *** as@alt-print.com,
**** juergen.eckert@unileoben.ac.at, ***** rostislavpodolskij@gmail.com

# RESIDUAL-STRESS FORMATION AND MITIGATION IN THE LPBF-MANUFACTURED AISI 316L STAINLESS STEEL: A REVIEW OF PROCESSING STRATEGIES AND HEAT-TREATMENT APPROACHES

Additive manufacturing of metal products using the laser powder bed fusion (LPBF) technology offers broad opportunities to produce parts with complex geometry from steels and alloys. At the same time, high temperature gradients and ultra-high cooling

Citation: G.A. Kononenko, P. Ramasamy, S.V. Adjamsky, J. Eckert, R.V. Podolskyi, O.A. Podolska, and S.I. Baduk, Residual Stress Formation and Mitigation in the LPBF-Manufactured AISI 316L Stainless Steel: A Review of Processing Strategies and Heat Treatment Approaches, *Progress in Physics of Metals*, **27**, No. 3: 568–604 (2026)

rates characteristic of LPBF lead to intensive formation of residual internal stresses, which negatively affect the geometric stability, mechanical properties, and operational reliability of products. The work provides a comprehensive review of recent national and international research on the mechanisms of residual-stresses' formation and mitigation in parts made of AISI 316L steel fabricated by means of the LPBF technology. Using network bibliographic analysis (VOSviewer) with the OpenAlex database and clustering by stacking (Gephi), key scientific directions, process parameters, and scanning strategies, which influence the stress–strain state of products decisively, are systematised. The roles of the geometry of the parts, the layer thickness, the laser energy density, the orientation, and size of the scanning fields in the formation of macro- and microstresses are analysed. Special attention is paid to the analysis of regulatory and technical documentation and to the heat-treatment modes of AISI 316L steel and its analogues, as well as to the generalisation of global experience in the application of thermal methods for relieving internal stresses for the LPBF products. As shown, heat treatment is the most effective tool for achieving a favourable level and distribution of residual stresses, while maintaining the required set of mechanical properties. The results obtained can be used to substantiate the rational parameters of the LPBF process and post-processing of AISI 316L steel parts for critical engineering applications.

**Keywords:** 316L steel, laser powder bed fusion, residual stresses, heat treatment, technological parameters.

## 1. Introduction

Additive manufacturing (AM) is a modern group of advanced technologies that enable the rapid and high-quality fabrication of components with complex and unique geometries that are difficult or impossible to produce using conventional manufacturing methods. Currently, research efforts are primarily focused on two major directions: the development of AM quality assurance systems [1–20] and the identification of new structure–property relationships in well-established materials traditionally processed by conventional routes [21–42].

Residual stresses are among the intrinsic features of metallic materials produced by layer-by-layer fusion using the laser powder bed fusion (LPBF) process. These stresses can significantly affect both the mechanical performance and dimensional accuracy of fabricated parts [43–46]. The accumulation of residual stresses generated during processing, caused by rapid localised heating and cooling cycles (cooling rates of approximately $10^3$–$10^8$ °C/s) [1], may result in distortion, cracking, or even premature component failure during service [47, 48]. Consequently, mitigating residual stresses is considered one of the most critical and challenging issues in the field of AM [1, 43, 47, 49]. Therefore, reducing the detrimental effects of residual stresses requires a fundamental understanding of their influence on the geometric stability and service properties of additively manufactured materials.

## 2. Materials and Methods

### *2.1. Materials and Processing*

This work, a network bibliographic analysis was applied using the VOSviewer software [50] and existing databases (OpenAlex) [51] to increase the accuracy of the search, narrow the scope of the search and provide a comprehensive analysis of the current state of the art in reducing internal stresses when using the LPBF technology by determining the number of publications with the largest number of identical keywords, their relationships with other keywords in accordance with the set goal of the study (review). As a result of analysing publications in the OpenAlex database, a dataset of 1524 publications (without time limits) was obtained. It should be noted that to achieve a more homogeneous clustering and to strengthen the focus on the processes and features of the LPBF technology, keywords indicating the speciality of research (materials science, computer science, *etc*.), research material and keywords that are the key combination of these clusters were excluded, namely, additive technologies, LPBF technologies, and LPBF processes.

Based on the results obtained, the keywords distributed by clusters according to the number of keywords from scientific publications were analysed in the specialised software package Gephi [52] using the classical stacking algorithm 'Fruchterman Reingold' with a speed of 100 units and an area covering all the main clusters for stacking. At the next stage, stacking modelling with attraction and linear repulsion was performed using the 'BearnsHut' approximation with automatically determined speed parameters, followed by defining the keywords selected for the analysis. As a result of the analysis, it was found that the average degree of the used keywords is 28, the diameter of the graph is 7, which indicates a high affinity of each bridge with the main keyword (high frequency of use in scientific works), and modularity is 0.263 (indicating that the keywords are divided into approximately 3 main clusters). As a result of the analysis of publications, it was established which keywords have the largest 'bridges' for minimising internal stresses in the LPBF technologies and are the most widely used in the scientific community (Fig. 1).

The experiments used prototypes manufactured on 3*D* printers equipped with ytterbium lasers and various focusing systems, including an F-Theta lens and a three-axis (dynamic) focusing system.

### *2.2. Structural Characterisation*

Microstructural investigations were performed on polished specimens prepared by mechanical grinding and polishing using an automatic polishing system (Struers Labopol-5) equipped with a LaboForce-3 rotating head. Grinding and polishing were carried out using magnetic-backed abrasive and polishing discs with progressively decreasing grit sizes to achieve a

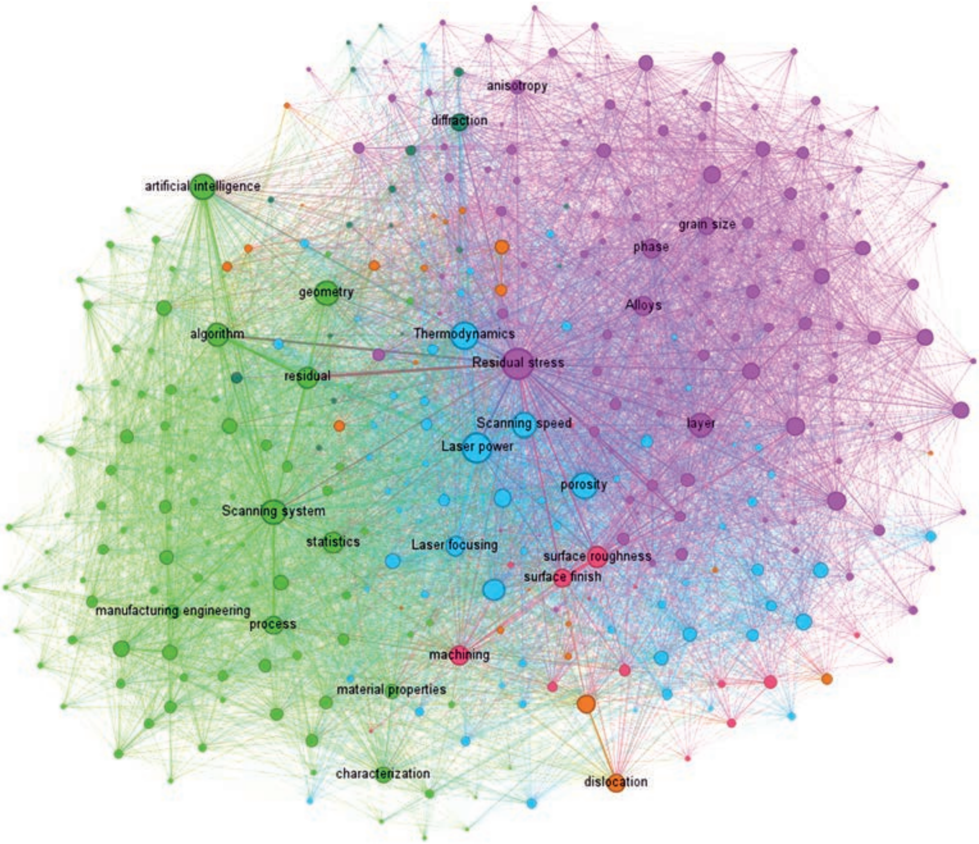


*Fig. 1.* Bibliometric map of research directions related to residual stress minimisation in the LPBF process

mirror-like surface finish. Various techniques were employed to reveal the microstructure of the investigated samples, including both chemical and electrochemical etching (Table 1).

Structural examination in the polished and etched conditions, as well as microstructural analysis, was conducted using optical microscopy in bright-field mode with Carl Zeiss AxioVert 200M and Neophot-32 microscopes.

## 3. Results and Discussion

In recent years, the production of metal products using the original CAD model directly from electronic data based on layer-by-layer manufacturing has evolved from rapid prototyping to AM [54–56]. In contrast to traditional manufacturing technologies, AM offers much greater design freedom. For the first time, product design is no longer strictly limited by manufacturing methods; individual parts with high complexity, such as honeycomb structures, complex internal structures, or cooling channels, can be implemented without adhering to specific design rules. In addition, parts designed using computer-aided design (CAD) technology can undergo topology optimisation [53] and be implemented without additional costs for technological equipment or manufacturing operations. This provides many advantages, including complex geometry, weight reduction, shorter order execution time, waste reduction, and functional integration. In the LPBF, metal is exposed to a laser, which melts it. When the metal cools, compressive stresses develop, which can cause a change in the products' initial shape (warping) [57–63]. The metal structure of parts manufactured using the LPBF technology features a fine-grained structure, layering, and texture oriented along the growth or construction direction. In addition, such products are prone to the occurrence of internal stresses due to temperature gradients and complex geometry, such as the transition from a large cross-section to a small one. The presence of internal stresses can lead to a decrease in strength, corrosion resistance, fatigue strength and resistance to corrosion cracking. Therefore, for parts made of AISI 316L steel manufactured using the LPBF technology, it is necessary to develop measures to prevent the formation and reduce residual stresses.

Usually, heat treatment is used to achieve the final combination of mechanical properties and structural state, but the modes should take into account not only the chemical composition but also the initial structure before heat treatment. For products manufactured using the LPBF tech-

*Table 1*. **Methods for preparing test sections by electrochemical polishing and chemical etching [53]**

| Chemical etching of the structure | | | | |
|---|---|---|---|---|
| Material | Name | Composition | Purpose | Exposure time, s |
| 316L | Kulling reagent No. 2 | 5 g $CuCl_2$, 100 ml HCl, 100 ml $C_2H_6O$ | Used at room temperature; reacts quickly with ferrite, but very slowly with austenite | 2 |
| | Marble Reagent | 4 g $CuSO_4$, 20 ml HCl, 20 ml $H_2O$ | Actively interacts with the σ-phase; to detect twinning | 10 |
| Electrochemical polishing | | | | |
| Material | Electrolyte | Voltage, V | Current density, A/cm$^2$ | Temperature, °C |
| 316L | $H_3PO_4$ 85%, $C_3H_8O_3$ 99%, distilled water | 19–28 | 7.5 | 60–90 |

nology, which have a different initial structure after construction compared to traditional production, it is impossible to apply the same modes without taking into account the specified features of the metal structure. The influence of heat treatment parameters on residual internal stresses in a part made of AISI 316L steel manufactured using the LPBF is insufficiently studied. Thus, there is a need for a detailed study of the influence of heat treatment on mechanical properties and the reduction of internal stresses, taking into account the manufacturing method and the initial structural state of parts made of AISI 316L steel.

### 3.1. Analysis of Current Standards and Technical Regulations

AISI 316L stainless steel, due to its high corrosion resistance and strength, is used in many industrial sectors. AISI 316L steel also meets hygiene requirements; it is used in the chemical, food, pharmaceutical, and medical sectors, as well as in the oil refining, mining, pulp and paper, machine-building industries, in construction, and architecture.

AISI 316L steel has good technological properties and is easily deformed, so a wide range of metal products are made from it, including pipes, sheets, and profiles.

AISI 316L is a steel grade that is AISI 304 steel, improved by adding about 2.5% molybdenum. Thanks to molybdenum, this grade of steel is particularly resistant to corrosion, high temperatures, and aggressive environments. AISI 316L steel is used in the production of equipment and products that operate in aggressive environments, such as, for example, seawater of cold seas, and in acid solutions (sulphuric, alkaline, phosphoric, citric, lactic, *etc.*). It is also used to manufacture meshes for straight and oblique coarse filters, as well as dishes, cutlery, tanks, and containers. It should be noted that this steel grade has several analogues, namely, 03X16H15M3 (CIS), 1.4435, 1.4429 (EU), X2CrNMo18-14-3, X2CrNiMoN17-13-3 (Germany), SUS F 316L (Japan), Z2CND17-13 (France), AISI 316L (USA) (Table 2).

As a result of the analysis of the requirements for the chemical composition, it was found that the standards DIN EN 10253-3 (X2CrNMo18-14-3, X2CrNiMoN17-13-3), EN 10253-3 (1.4435, 1.4429), ASTM A240 (AISI 316L), and AFNOR NFA EN 10216-5 (Z2CND17-13) regulate the presence of nitrogen. It should be noted that the standards AFNOR NFA EN 10216-5, ASTM A240, JIS G 3214, and GOST 5632 regulate within the brand by 1% more nickel and by 1% less chromium compared to the standards DIN EN 10253-3 and EN 10253-3 to minimise the content of δ-ferrite, or reduce intergranular corrosion.

In addition to chemical content, the standards regulate mechanical properties, and the requirements are presented in Table 3. When analysing the requirements for mechanical properties, it was found that the

*Table 2.* **Chemical composition of AISI 316L steel and its analogues (wt.%)**

| Material | C | Si | Mn | P | S |
|---|---|---|---|---|---|
| 03X16H15M3 | <0.03 | <0.4 | 1.0–2.0 | <0.02 | <0.03 |
| 1.4435 | <0.03 | <1.0 | <2.0 | <0.045 | <0.015 |
| 1.4429 | <0.03 | <1.0 | <2.0 | <0.045 | <0.015 |
| X2CrNMo18-14-3 | <0.03 | <1.0 | <2.0 | <0.045 | <0.015 |
| X2CrNiMoN17-13–3 | <0.03 | <1.0 | <2.0 | <0.045 | <0.015 |
| SUS F 316L | <0.03 | <1.0 | <2.0 | <0.04 | <0.03 |
| Z2CND17-13 | <0.03 | <1.0 | <2.0 | <0.04 | <0.015 |
| AISI 316L | <0.03 | <0.75 | <2.0 | <0.045 | <0.03 |

*Table 3.* **Mechanical properties of AISI 316L stainless steel and its analogues**

| Material | Country | Standard | UTS, MPa | YS, MPa | Elongation, % | Narrowing, % | Hardness, *HB* | *KCV*, J |
|---|---|---|---|---|---|---|---|---|
| 03X16H15M3 | CIS | GOST 5949 | ≥490 | ≥196 | ≥40 | — | — | — |
| 03X16H15M3 | CIS | GOST 7350 | ≥490 | ≥196 | ≥40 | — | — | — |
| 1.4435 | EU | EN 10253-3 | 490–690 | ≥200 | ≥35 | — | ≤200 | (≥100) |
| 1.4429 | EU | EN 10253-3 | 580–800 | ≥220 | ≥40 | — | ≤220 | (≥100) |
| X2CrNMo18-14-3 | Germany | DIN EN 10253-3 | 490–690 | ≥200 | ≥35 | — | ≤200 | (≥100) |
| X2CrNiMoN17-13-3 | Germany | DIN EN 10253-3 | 580–800 | ≥220 | ≥40 | — | ≤220 | (≥100) |
| SUS F 316L | Japan | JIS G 3214 | ≥480 | ≥175 | ≥29 | ≥50 | ≤187 | — |
| Z2CND17-13 | France | AFNOR NFA EN 10216-5 | 490–690 | ≥190 | ≥40 | — | — | (≥100) |
| AISI 316L | USA | ASTM A312 | ≥485 | ≥170 | ≥35 | — | — | — |

ASTM A312, JIS G 3214, GOST 7350, GOST 5949 standards regulate the tensile strength with a minimum permissible value (≅485 ± 5 MPa), while the EN 10253-3, DIN EN 10253-3, AFNOR NFA EN 10216-5 standards regulate the value of this characteristic in the range (490–690 and 580–800 MPa, respectively). However, it should be noted that the yield strength according to the ASTM A312 standard must be ≥170 MPa, according to the JIS G 3214 — ≥175 MPa, and GOST 7350, GOST 5949, and AFNOR NFA EN 10216-5 regulate the yield strength level ≥ 190 MPa. Standards EN 10253-3 and DIN EN 10253-3 specify a minimum yield strength of 200 MPa, which generally indicates high strength.

The final set of mechanical properties is obtained through heat treatment of rolled steel [65–70]. Based on this statement, an analysis of regulatory and technical documentation was conducted to determine the regulated heat-treatment modes for AISI 316L steel and its analogues (Table 4).

| | Cr | Ni | Mo | N | Fe | Ref. |
|---|---|---|---|---|---|---|
| | 16.8–18.3 | 13.5–15.0 | 2.2–2.8 | — | Rest | [65] |
| | 17.0–19.0 | 12.5–15.0 | 2.5–3.0 | ≤0.11 | Rest | [66] |
| | 17.0–19.0 | 12.5–15.0 | 2.5–3.0 | 0.12–0.22 | Rest | [66] |
| | 17.0–19.0 | 12.5–15.0 | 2.5–3.0 | ≤0.11 | Rest | [67] |
| | 17.0–19.0 | 12.5–15.0 | 2.5–3.0 | 0.12–0.22 | Rest | [67] |
| | 16.0–18.0 | 12.0–15.0 | 2.0–3.0 | — | Rest | [68] |
| | 16.5–18.5 | 11.0–14.0 | 2.5–3.0 | ≤0.11 | Rest | [69] |
| | 16.0–18.0 | 10.0–14.0 | 2.0–3.0 | <0.1 | <0.03 | [70] |

*Table 4*. **Heat treatment regimes of 316L stainless steel and its analogues according to regulatory and technical standards**

| Material | Country | Standard | Heat treatment |
|---|---|---|---|
| 03X16H15M3 | CIS | GOST 5949 | Solution treatment at 1070–1100 °C, followed by air or water cooling |
| 03X16H15M3 | CIS | GOST 7350 | Solution treatment at 1080–1100 °C, followed by air or water cooling |
| 1.4435 | EU | EN 10253-3 | Solution treatment at 1020–1100 °C, followed by air or water cooling |
| 1.4429 | EU | EN 10253-3 | Solution treatment at 1020–1100 °C, followed by air or water cooling |
| X2CrNMo18-14-3 | Germany | DIN EN 10253-3 | Solution treatment at 1020–1100 °C, followed by air or water cooling |
| X2CrNiMoN17-13-3 | Germany | DIN EN 10253-3 | Solution treatment at 1020–1100 °C, followed by air or water cooling |
| SUS F 316L | Japan | JIS G 3214 | Solution treatment at 1010–1150 °C, followed by water quenching |
| Z2CND17-13 | France | AFNOR NFA EN 10216-5 | Solution treatment at 1020–1120 °C, followed by water quenching |
| AISI 316L | USA | AMS 2759/4B [71] | Solution treatment at 1093 °C, followed by air, oil, water, or polymer quenching |
| AISI 316L | USA | AMS 2759/4B [71] | Tempering at 427 °C, followed by air cooling |
| AISI 316L | USA | AMS 2759/4B [71] | Stress relief at 899 °C, followed by water quenching |

According to the results of the NTD analysis, it was established that the heat treatment of steel analogues 03X16N15M3, 1.4435, 1.4429, X2CrNMo18-14-3, X2CrNiMoN17-13-3, SUS F 316L, Z2CND17-13 according to the standards GOST 5949, GOST 7350, EN 10253-3, DIN EN 10253-3, JIS G 3214, AFNOR NFA EN 10216-5 includes hardening from temperatures above 1000 °C. Unlike the previous ones, the AMS 2759/4B standard includes several heat treatments that meet the above requirements, including a heat treatment to relieve internal stresses: heating to 899 °C with subsequent cooling in water. Also, the AMS 2759/4B standard specifies the holding time at a temperature that depends on the cross-section of the processed part.

From the above, it follows that AISI 316L steel is used for products operating in aggressive environments and under high loads; that is, it has a wide range of applications and numerous analogues. The progressive modern LPBF production method is promising for use across various industries and enables the manufacture of products with complex shapes. However, the LPBF products are prone to internal stresses due to temperature gradients and complex geometry. Heat treatment modes for parts manufactured using the LPBF technology should ensure the formation of the final complex of mechanical properties, structural state, favourable level, and distribution of residual stresses.

### 3.2. Residual Stresses

Internal residual stresses in polycrystalline materials are classified into three main classes, namely stresses of the first kind (macro-stresses), of the second kind (microstresses), and of the third kind (intracrystalline residual stresses) [72–73]. Macrostresses are balanced in the volume of the entire test specimen or product. The orientation of these stresses is, in most cases, related to the geometry of the product. Reaching macrostresses of the stress level causes deformation (warping (Fig. 2, *a*) and cracking (Fig. 2, *b*)) of the product [1, 72]. Even more dangerous is the ability of macrostresses to manifest later, when, after processing, the finished part of the mechanism begins to wear out suddenly and quickly due to dimensions exceeding the tolerance limit.

Microstresses vary within individual grains and crystal cells; in most cases, this is associated with crystal anisotropy, the orientation of crystallographic planes, and the presence of other phases [75]. Intracrystalline residual stresses are associated with the inhomogeneous microstructure in the grain, such as dislocation centres inside the grains [76]. In general, microstresses arise after material processing and gradually develop under the applied load. Figure 3 presents various types of residual internal stresses in polycrystalline materials. It should be noted that the issue of residual internal stresses was also paid attention to in the traditional pro-

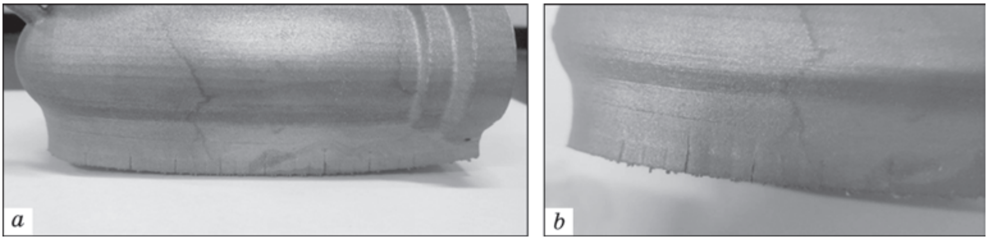


*Fig. 2*. Macrostress-induced part defects: distortion (*a*), cracking (*b*)

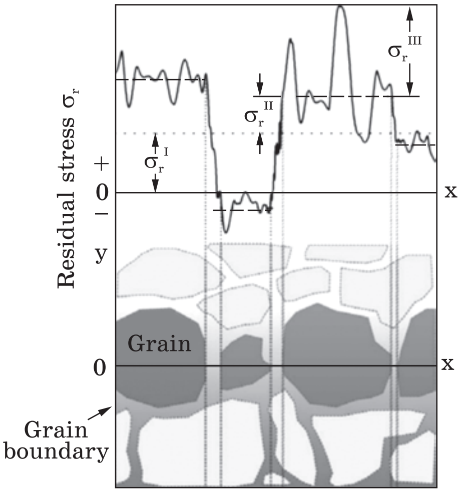


*Fig. 3*. Schematic illustration of the hierarchy of residual stresses in polycrystalline materials: $\sigma^{I}$ (macroscopic stresses), $\sigma^{II}$ (intergranular or microstresses), and $\sigma^{III}$ (intragranular or crystallographic stresses) [77]

duction method, but mainly in relation to macrostresses in parts after the processes of rolling, thermal annealing, or mechanical treatment. The reasons for the formation of internal stresses in the LPBF products are the high cooling rate during solidification of the melt bath within one track (cooling rates from $10^3$ to $10^8$ °C/s) and a large temperature gradient between the liquid melt of the bath and the previous solid layers of the product [1, 78–80]. This is especially true for steels and alloys [1], which have low heat-transfer coefficients. The uneven distribution of residual stresses is associated with differences in the cooling conditions of the track that forms the side surface of the part and the track in the centre of its cross-section, which leads to different heat removal at the powder-metal and metal–metal interfaces, respectively. Figure 4 schematically depicts the effect of heat supply on the formation stress gradient in individual layers during heating and cooling during the LPBF process.

As a result of the above thermal effect, the next part of the layer is subjected to tensile forces while the previously deposited layer is subjected to compressive stresses. Thus, this problem arises when subsequent melt–pool layers limit the thermal expansion and contraction of the layers directly below them. It should be noted that this effect can occur simultaneously at the depth of several layers, thus causing elastic deformation within the layers, which will lead to the emergence of a stress gradient between the layers [78, 81]. Figure 5 [79] shows a diagram illustrating this effect graphically. Thus, it has been established that the internal re-

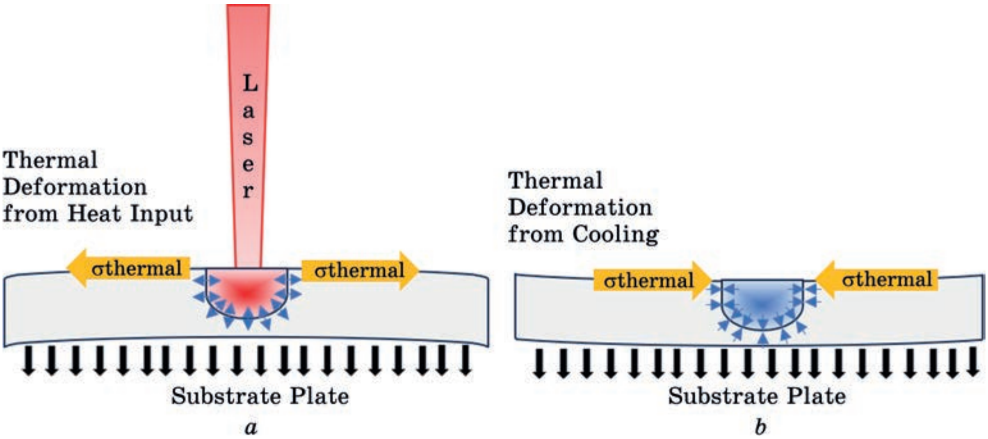


*Fig. 4*. Schematic illustration showing the effect of heating (*a*) and cooling (*b*) on the residual stress gradient during the LPBF process [78, 79]

sidual stresses are influenced by many manufacturing parameters, such as the number and thickness of layers [78], geometry, scanning strategy [82–85], and laser energy density [86].

Layers, depending on the geometry, are divided into zones; each zone is assigned an individual identifier, according to which the trajectories of movement are constructed, and the types of tracks with their parameters of power and speed of movement of the laser beam are established. These identifiers can be divided into three main groups: the lower layer (down-skin), the inner layer (in-skin), and the upper layer (up-skin) (Fig. 6, *a*). At the same time, each group has its own subgroups: hatches, contour (border), and post-contour (fill border), as shown in Fig. 6, *b*. Laser hatching, or the laser beam movement strategy, is the trajectory of the laser beam along the surface of the metal powder layer when pouring the main body and product contours [87]. In the LPBF process, a temperature gradient develops from the upper layer to the previous layer, causing grains to grow along the direction of heat flow and determining the priority direction of grain growth. Thus, one direction becomes the main direction of grain growth after the layer solidifies. Therefore, the laser scanning strategy significantly affects the texture of the manufactured product using the LPBF [88].

Some features of the geometry of the parts (overhanging edges, inclined surfaces, thin walls, thin profile, variable cross-section, holes) require special scanning conditions, for example, double bypassing the contour of the thin profile, redistribution of laser energy in the beam, and also, possibly, changing the power and scanning speed of the laser beam.

Almost all advanced processes for manufacturing parts, which seek to improve their quality, focus on minimising the effects of internal stresses [89].

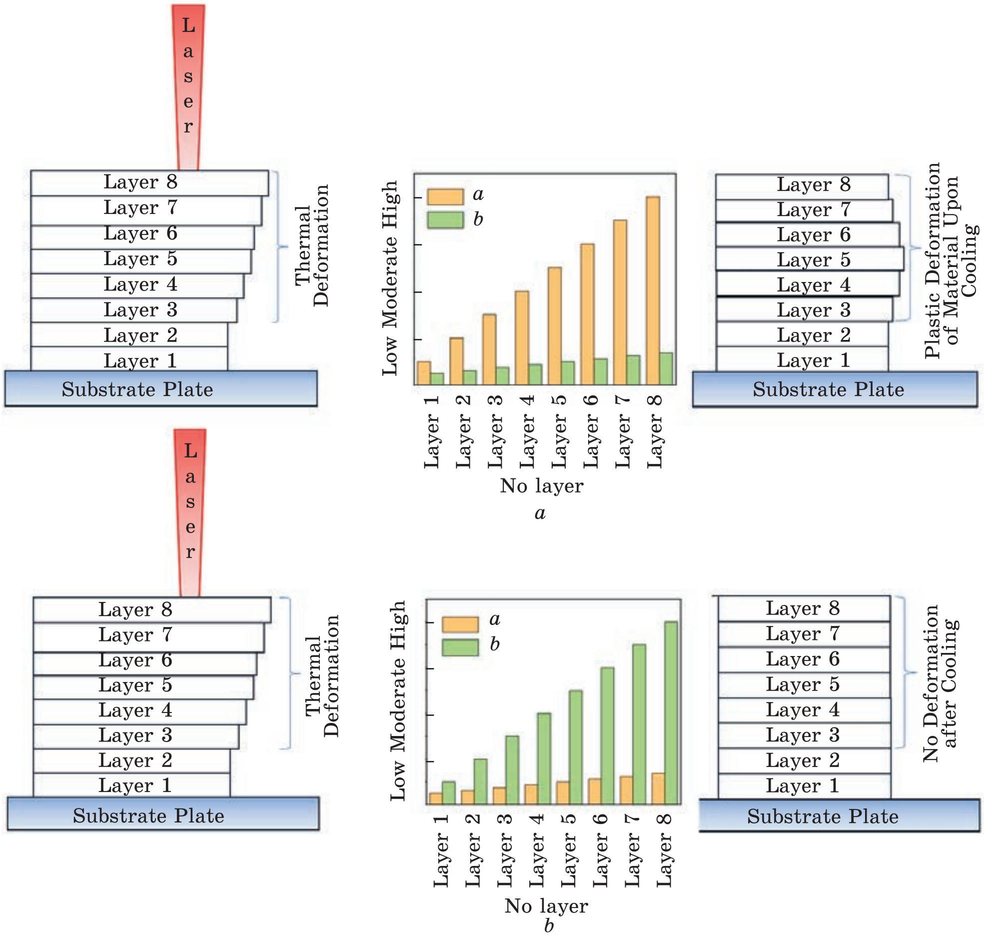


*Fig. 5*. Schematic representation of interlayer stress evolution: (*a*) thermally induced stresses between layers; (*b*) thermally induced deformation within layers; (*c*) unconstrained (sliding) layers fixed to the substrate; (*d*) metallurgically bonded layers rigidly constrained by the build plate [79]

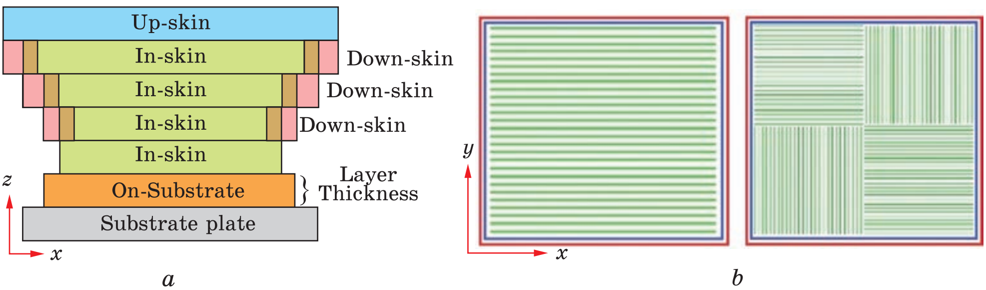


*Fig. 6*. Layer formation along the build direction (*a*) and subgroups of scan tracks (*b*) [90]

### 3.3. Systematisation of Established Approaches to Residual Stress Reduction in the LPBF

As a result of the material behaviour of samples printed using different construction strategies, tensile or compressive stress regions form, as shown in a true-tension diagram (Fig. 7), which shows the relationship between elongation and stress. When the yield point is exceeded, the metal demonstrates plastic behaviour, characterised by irreversible plastic deformation, and the dependence of deformation on stress becomes nonlinear.

In the formation of residual stresses, in addition to high cooling rates and the constant proximity of liquid and solid metal during the construction of the part, the uneven distribution of residual stresses associated with the geometry is important: the presence of protruding parts, transitions from thick to thin sections, acute-angled elements, and holes.

When manufacturing parts using the LPBF technology, stresses arise in the contour (edge) area of a massive product, which can lead to the formation of some defects [91]: changes in the initial shape (distortion) of the product [92] (Fig. 8, *a*), the formation of pores and delamination (Fig. 8) between the new and cooled metal due to changes in its geometry, the appearance of microcracks (Fig. 9), the formation of a pronounced texture, which leads to a decrease in mechanical properties and their anisotropy.

### 3.4. Strategies for Minimising Residual Stresses via Control of Processing Parameters

In this regard, it is important to minimise residual stresses during the LPBF part manufacturing. To prevent deviations in the parts' geometry, it is necessary to account for the relationship between the supplied spe-

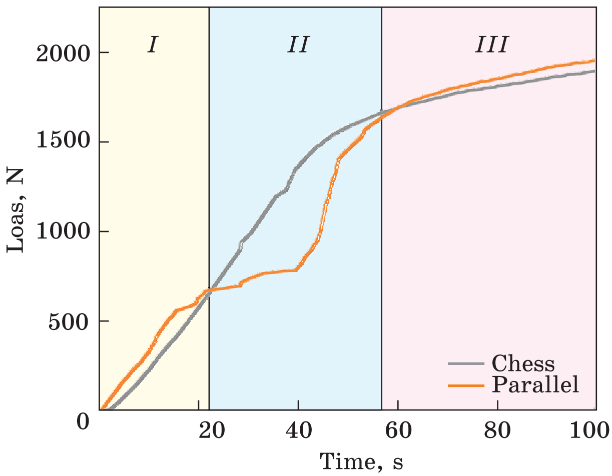


*Fig. 7.* True stress–strain curves of specimens produced using parallel and chessboard scanning strategies: *I* — proportional (elastic) region; *II* — yielding region; *III* — strain-hardening region [49]

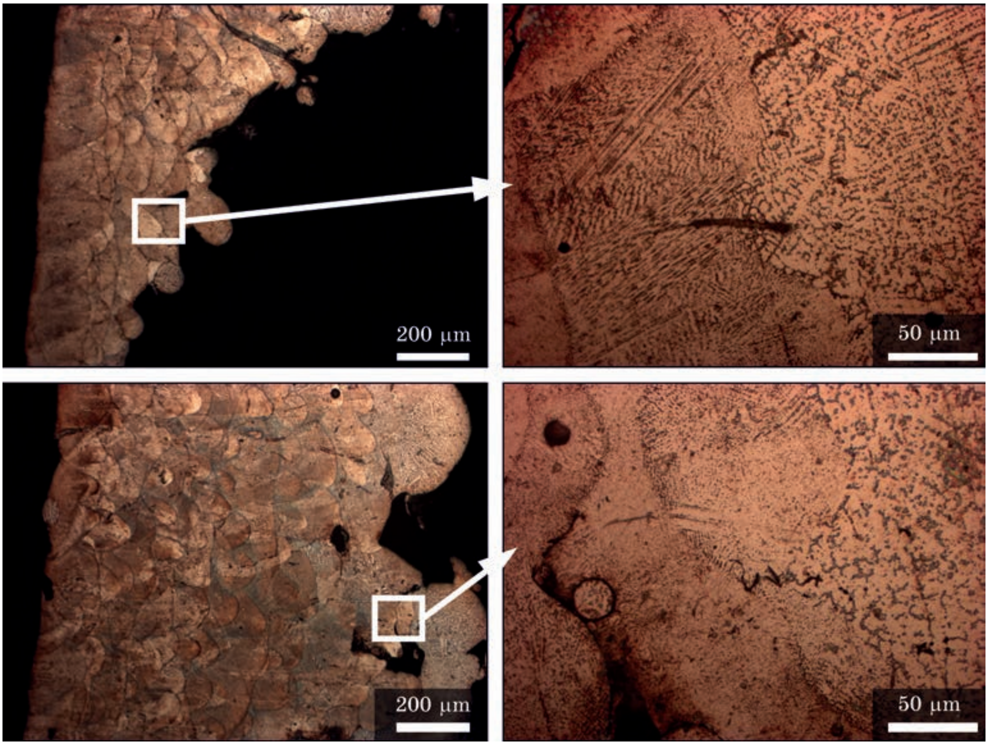

*Fig. 8*. Microstructural investigation of the delamination region

cific energy density and its absorption during the process [93]. However, the optimal technological parameters [49] and construction strategies [90, 94, 95] for the LPBF process on polycrystalline materials are difficult to predict, as product quality depends on numerous factors. Finding ways to pre-estimate and develop measures to reduce residual stresses in the manufacture of parts using the LPBF technology is a relevant task of modern materials science. The modern approach is to use rational parameters and scanning strategies while also taking into account the impact on defect formation and microstructure [1, 49, 96]. An alternative approach is to use heat treatment to remove internal stresses, thereby reducing their magnitude and subsequent impact [97]. The application of heat treatment should also be balanced with regard to the cost of production, the desired microstructure, and the required mechanical properties of the alloys.

If we consider the issue of minimising internal residual stresses while maintaining the required mechanical properties by controlling parameters and scanning strategies, there are several strategies for moving the laser beam within the layer being alloyed [94, 98–100] (Fig. 10).

Authors of the studies [95] changed the direction of the laser scanning in each new layer by a certain angle relative to the previous layer by 90°,

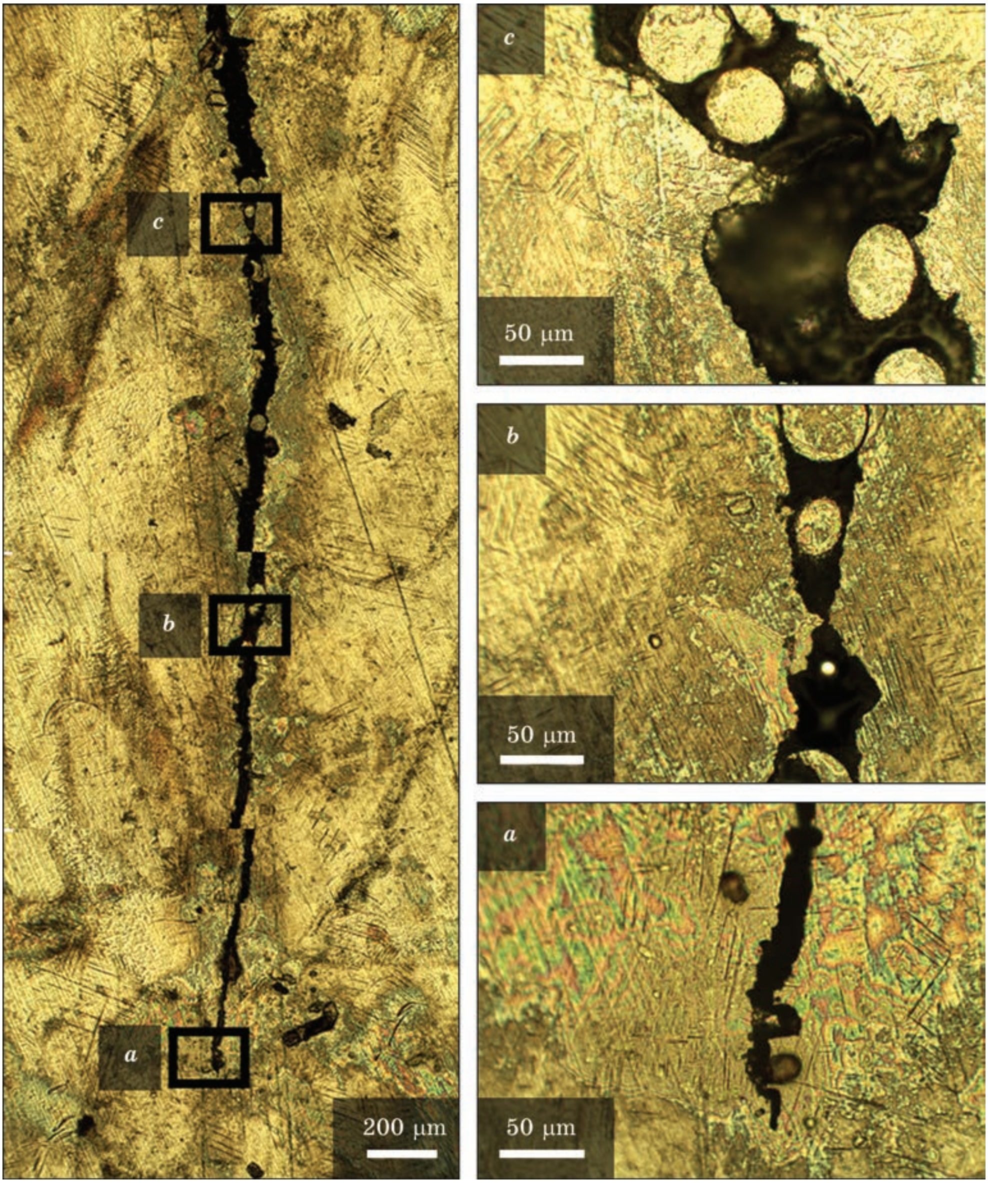


*Fig. 9.* Microstructural investigation of the component in the crack region

105°, 120°, 135°, 150° (Fig. 11). The best mechanical properties were in the objects obtained at a rotation angle of 105°, when the layers with the same direction of movement of the laser beam were repeated only after 24 layers. The sample obtained at an angle of 90° has the lowest mechanical properties, but the differences among the samples do not exceed 10%. In addition, it is also recommended to change the scanning strategy for the

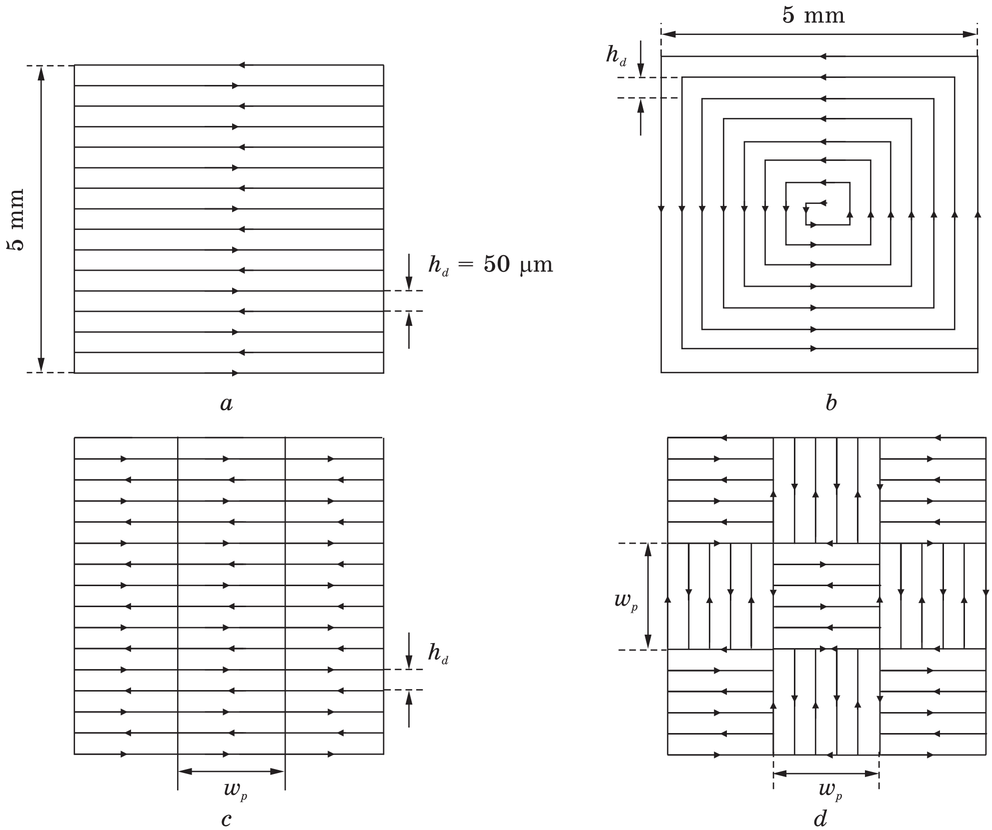


*Fig. 10.* Types of scanning strategies [94]: (*a*) parallel, (*b*) spiral, (*c*) alternating-direction parallel, and (*d*) chessboard (island)

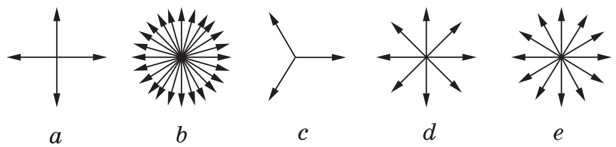


*Fig. 11.* Melting strategy: rotation angle between successive layer scan directions of 90° (*a*), 105° (*b*), 120° (*c*), 135° (*d*), and 150° (*e*); number of layers between identical scan directions: 4 (*a*), 24 (*b*), 3 (*c*), 8 (*d*), and 12 (*e*) [95]

lower (at the base of the platform), middle, and upper layers, since the heat dissipation conditions will be different everywhere.

As a result of these studies, the authors found that the scanning strategy plays an important role in determining mechanical properties, but internal stresses were not considered.

Authors of Ref. [96] conducted a study on a simple figure (prism) with dimensions of 24×46×21 mm, made of 316L steel, to determine the distribution of internal stresses at an average height by applying the x-ray dif-

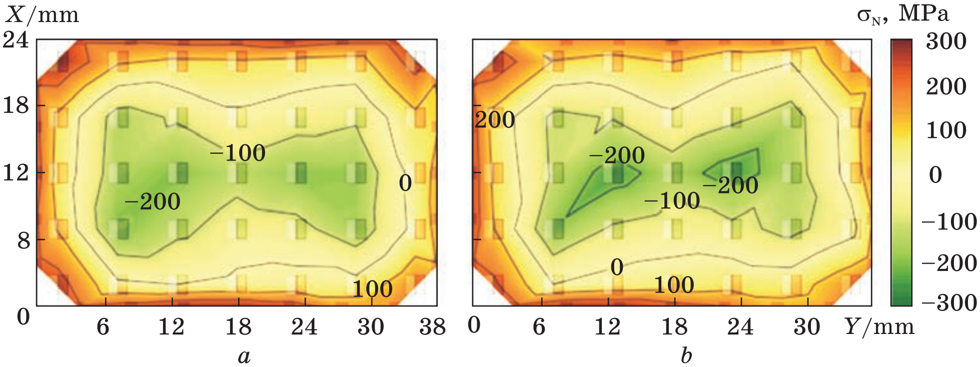


*Fig. 12*. Residual stress distribution along the build direction using a spiral scanning strategy: (*a*) from the centre toward the boundaries; (*b*) from the boundaries toward the centre [97]

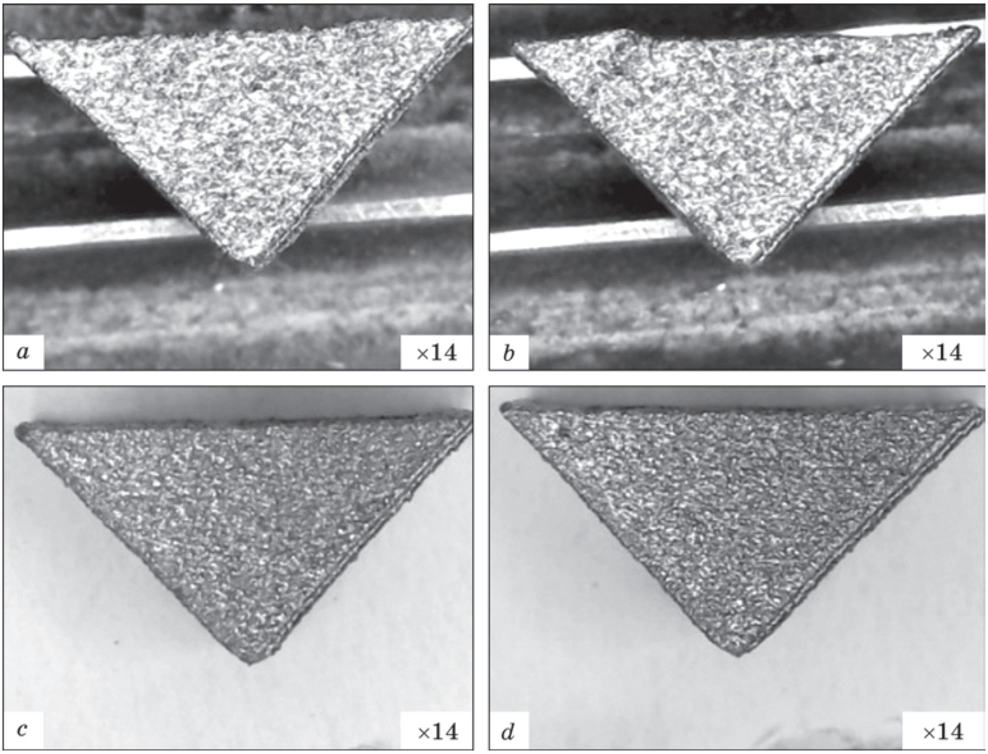


*Fig. 13*. Visual assessment of deformation in the experimental specimens: linear (straight-line) scanning (*a*, *b*); chessboard (island) scanning (*c*, *d*) [49]

fraction method. Within the framework of these studies, 2 prisms were analysed, manufactured using different scanning strategies: the spiral scanning strategy (Fig. 10, *b*), with the filling direction from the boundaries to the centre and vice versa. As a result of these studies, the authors

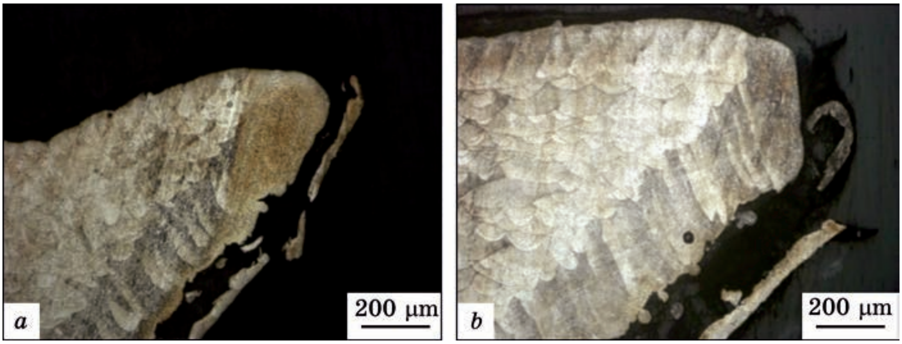


*Fig. 14*. Microstructural characterisation of the thin-edge zone of the specimens fabricated using different scanning strategies: straight-line scanning (*a*) and chess scanning (*b*) [49]

[96, 101] found that for the two scanning strategies, a similar distribution of internal tensile stresses was observed along the edges and compressive stresses along the centre. This distribution is characterised by compressive internal stresses within the volume, balanced by tensile stresses on the surface (Fig. 12).

Authors of Refs. [1, 49] believe that some possibilities are provided for minimising internal stresses, when implementing the LPBF technology: changing the geometry of the CAD model and controlling the process parameters, such as changing the size of the focal spot, using different types of tracks, rotating and shifting layers relative to the previous ones, and different printing strategies. In this work, the authors were guided by the statement of the authors of Ref. [80] that the influence of large temperature gradients can lead to high values of internal stresses, which can reduce mechanical properties such as strength, plasticity and fatigue life. The material of the sample built using the staggered scanning strategy transitions more smoothly into the self-hardening region; thereby, the rearrangement of the crystal lattice occurs at a higher load, which preserves the margin of transition to irreversible changes in the material. At stresses less than the yield point, the body can return to its original shape and size when the tensile stresses are removed [102].

When visually assessing the deformation (changes in the geometry of the samples) as a result of the action of residual stresses, the authors [49] noted that with a rectilinear printing order with a rotation of the layers relative to the previous one by 67° (Fig. 13, *a*), due to the stress, there is a greater curvature of the boundary in the thin edge region compared to samples, built under the same conditions, but in a staggered order (Fig. 13, *b*).

The microstructure of the experimental samples manufactured with different process parameters and printing strategies is presented in Fig. 14. It should be noted that the samples did not exhibit defects in the main body (porosity, high roughness). The formed melt pool of the main body under the influence of laser radiation, by melting the powder layer and the substrate material, has uniform melting and clearly constructed tracks.

As a result, the authors of Ref. [49] concluded that in samples printed with the strategy of building tracks in a checkerboard pattern (Fig. 10, *d*) with a rotation of 67°, less distortion was observed than in samples with a straight-line strategy (Fig. 10, *a*) of printing with a rotation of 67°.

Authors of Ref. [103] characterised the internal stresses in Inconel 718, manufactured using different scanning strategies with different checkerboard sizes (Fig. 10, *d*): 2×2 mm, 3×3 mm, 5×5 mm and 7×7 mm (22 samples). As a result, the sample with a checkerboard size of 2×2 mm had the lowest residual stresses; however, the presence of a crack limited its use. The formation of cracks was explained by the release of internal stresses.

As a result, the authors [103] found that due to the strong influence of temperature gradients, the dependence of internal stresses on the scanning strategy during LPBF manufacturing requires further systematic investigation.

The authors of [83] conducted a study on 316L steel intending to determine the influence of residual internal stresses caused by AM features. Within the framework of these studies [83], the authors used a comprehensive approach to analyse macrostresses, namely, using digital image correlation (DIC) analysis [104–106] in combination with removal and sectioning of the working plate and a non-destructive method, namely, neutron diffraction [107–111]. As a result, the authors of Ref. [83] obtained good agreement between the two measurement methods. Regarding the effect of the scanning strategy on the internal stresses, it was found that the reduction of the residual internal stresses was achieved by reducing the size of the scanning field, increasing the field rotation to 45 degrees and increasing the applied energy per unit length (laser power/speed). Neutron diffraction measurements show that although the in-plane residual stresses are affected by the rotation of the scanning island, the axial residual internal stresses do not change. The authors of [83] explained this in-plane behaviour by the discrepancy between the largest thermal stresses (scanning direction) and the largest part size.

Authors of Refs. [99, 112–114] investigated the effect on internal residual stresses of changing the length and orientation of laser scanning vectors, performing pre- and post-scanning and field scanning, changing the layer thickness, heating the base plate and heat treatment of the final parts. The results showed that all these process modifications improved residual stress values, particularly by modifying the scanning parameters and reducing the temperature gradient through preheating the work plate. In Ref. [112], it was found that heat treatment led to a greater reduction in macrostresses (80%) than optimising the parameters for field scanning (36%).

The authors of Ref. [114] considered the effect of laser parameters, powder properties, environmental conditions, and preheating on the quality of the final parts. The authors of Ref. [99] investigated the influence of three main factors: thermal treatment of the part after printing (70% improvement), heating the powder layer during printing (40% improvement), and re-scanning each layer before printing the next one (55% improvement). Authors of Refs. [115, 116] suggested that the laser scanning scheme can be designed to control residual stresses so that they dissipate naturally or even provide material advantages for polycrystalline materials. Authors of Ref. [115] analysed the possibility of scanning each layer more than once (re-melting) and found that this additional operation significantly reduced residual stresses. Authors of Ref. [116] optimised production to reduce deformation in the fabricated metal layers. As a result of the research [116], a spiral scanning strategy (Fig. 10, *b*) and a spiral scanning strategy for the LPBF technology were developed, as it helps reduce molten-layer deformation more effectively.

As a result of the analysis of the works [1, 49, 94–120], it was found that during the manufacturing of parts using LPBF, tensile internal stresses develop on surfaces, which are balanced by compressive internal stresses in the volume. Since the research was carried out on samples of simple shape, the results obtained are difficult to compare with parts of products with complex geometric shapes, which exhibit significant changes in cross-sectional dimensions. However, it should be noted that the applied, developed and implemented parameters and scanning strategies allow balancing internal stresses while avoiding distortions and fractures. However, the authors of works [1, 49, 94–120] noted that the most suitable method for achieving a neutral stress state is heat treatment to remove internal stresses.

### 3.5. Heat Treatment for Residual Stress Minimisation in the LPBF-Manufactured Austenitic 316L Steel

Considering the fact that the heat treatment of 316L stainless steel manufactured by the LPBF technology is not described in the standards, and the material in terms of its structural state is somewhat different from the traditional one, in recent years some researchers have tried to find optimal conditions for minimising internal stresses.

Many researchers are investigating the heat treatment processes of 316L stainless steel [99, 121–132]. Based on their studies, the mechanical properties listed in Table 6 were determined.

It should be noted that the main task of the authors of the works [121–126, 128–130] was not to minimize internal stresses, but to obtain the required level of mechanical properties in accordance with the EN 10216-5:2013 standard [121] and ASTM A240/A240M [122], determining the influence of various post-treatment methods on porosity, microstructure, mechanical properties and fracture mechanisms [123–126, 128–130].

It should be noted that some heat treatment modes presented in Table 5 are in the range of ±30–50 °C, which is regulated by the AMS 2759/4B standard [71]. Thus, it can be said that the authors of the works [121–124, 127, 128, 131, 132], when choosing heat treatment parameters, were guided by the standard [71].

If we consider the issue of reducing internal stresses in more detail, the authors of [131, 132] carried out heat treatment at temperatures of 400, 650, and 800 °C to remove internal stresses in a muffle furnace with a protective environment (argon), as a result of Ref. [131], they achieved a reduction in internal stresses by 23%, 65%, and 90%, respectively. This result was fully confirmed in Ref. [132], where the removal of internal stresses using similar heat treatment in a protective environment of argon was achieved by 31.3%, 67.4% and 93.2%, respectively. However, it

*Table 5.* **Mechanical properties of AISI 316L stainless steel after stress-relief heat treatment**

| Temperature, °C | Time, min | UTS, MPa | YS, MPa | Elongation, % | Hardness, *HV* | *A*, J | Ref. |
|---|---|---|---|---|---|---|---|
| 600 | 120 | 660 | 495 | 25 | 271±25 | 120 | [121] |
| 950 | 120 | 580 | 360 | 44 | 215±14 | 152 | [121] |
| 1095 | 120 | 600 | 350 | 50 | 212±20 | 120 | [121] |
| 1100 | 20 | | | | 169±6 | | [122] |
| 1050 | 20 | | | | 132±3 | | [122] |
| 1150 | 20 | | | | 133±7 | | [122] |
| 800 | 10 | | | | 140±6 | | [122] |
| 900 | 120 | 595 | 370 | 29 | | | [123] |
| 900 | 120 | 582 | 365 | 31 | | | [123] |
| 900 | — | 674 | 419 | 51 | | | [124] |
| 1150 | 180 | 426±13 | 201±4 | 38±6 | | | [125] |
| 1095 | 60 | 635±17 | 375±11 | 51±3 | | | [126] |
| 650 | 120 | 617±1.4 | 475 | 54.1±1.6 | | | [127] |
| 388 | 240 | 717 | 496 | 28 | | | [127] |
| 1050 | 120 | 673±13 | 424.6 | 44.3 | | | [128] |
| 1200 | 120 | 684±16 | 416±9 | 52±3 | | | [129, 130] |
| 400 | 240 | 574.4±0.7 | 418.3±2.2 | 45.8±1.6 | | | [131, 132] |
| 650 | 120 | 550.5±2.0 | 365.8±2.0 | 38.1±0.9 | | | [131, 132] |
| 800 | 120 | 536.7±5.5 | 327.3±2.2 | 32.5±1.6 | | | [131, 132] |
| 1100 | 5 | 554.6±4.6 | 311.9±2.5 | 57.5±2.0 | | | [131, 132] |
| 1100 | 30 | 546.1±2.3 | 307.8±3.0 | 51.5±1.3 | | | [131, 132] |
| 1100 | 480 | 558.8±2.3 | 293.5±7.6 | 50.5±0.6 | | | [130, 131] |
| 1400 | 10 | 535.3±2.2 | 232±2.7 | 43.3±0.2 | | | [130, 131] |

should be noted that, as a result of microstructural studies, it was found that after high-temperature heating, there was a growth of columnar grains and an increase in the size of inclusions. The study focused on assessing the microstructure and corrosion behaviour of 316L steel after heat treatment. The authors of [129, 130] chose two temperature regimes, namely 650 °C and 1050 °C, with the temperature for 30 min and holding for 30 min in an argon atmosphere, with cooling in the furnace. The regime using the holding at a temperature of 650 °C was determined in Ref. [130] as relieving internal stresses; at this temperature, the structure does not undergo significant changes, in contrast to heat treatment at a temperature of 1050 °C.

Authors of Ref. [99] applied heat treatment at 600 and 700 °C for 1 hour; these heat treatment parameters reduced residual stresses by 70%.

During the experiment, the authors of Ref. [133] conducted heat treatment in a vacuum using the following parameters: heating to 1030 °C for 1 hour, followed by forced cooling with nitrogen. As a result of the heat treatment, internal stresses were reduced by up to 40%. Within the framework of the studies conducted by the authors of Ref. [134], 3 temperature regimes were applied: holding at 400, 800, and 1200 °C for 1 hour. As a result, the dislocation structure remained stable up to 400 °C. At 800 °C, no distortions were detected at the grain boundaries. Similarly, after heat treatment at 800 °C, grain-boundary segregation of elements was no longer detected. During deformation at the grain boundaries of samples annealed at 400 and 800 °C, an accumulation of additional deformation at the macro level was recorded compared to the undeformed state. The results demonstrate that even a weak array of dislocations along the grain boundary can successfully pin dislocations, although with a reduced ability to coexist with dislocations and individual structures found in the microstructures of finished and annealed samples at 400 °C. In addition, the authors of Ref. [135] applied a heat treatment with the following parameters: heating to 600 °C for 4 hours to determine the effect of heat treatment on removing internal stresses and on the value of the endurance limit. The study found that this heat treatment reduced internal stresses by 46%.

In the context of Ref. [136], the authors examined in greater detail the influence of heat treatment parameters. Experimental heat treatments were carried out at different temperatures (650–800 °C with a step of 50 °C), holding times (4–8 hours with a step of 2 hours), and in the range of cooling rates ≈0.15–0.19 °C/s. As a result of the studies conducted by the authors, it was concluded that holding time plays a major role in minimising internal stresses; samples that were subjected to holding for 6–8 hours experienced a more uniform levelling of the stress state. However, it should be noted that when the temperature increases above 700 °C, recrystallization occurs with subsequent growth of austenite grains. In general, the authors of Ref. [136] concluded that the stress state achieved, close to

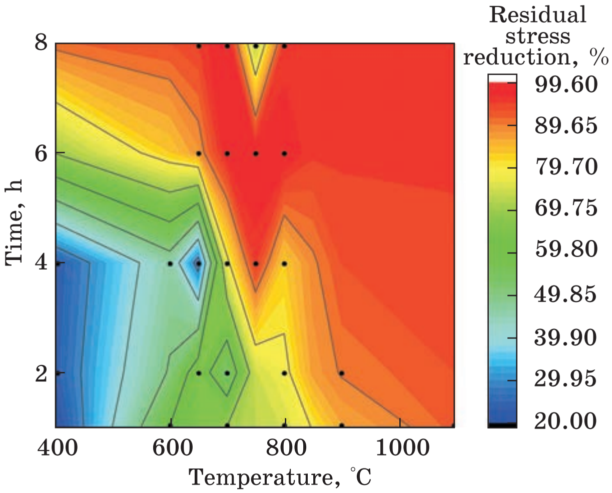


*Fig. 15.* Relationship between residual stress reduction and heat-treatment parameters (temperature and holding time) in 316L stainless steel, compiled from the data reported in Refs. [98, 121–141]

zero during subsequent heat treatment, further reduced the internal stresses of the areas that were close to zero, thus achieving the bending effect. It should be noted that many authors [137–141] are conducting research to reduce internal stresses. Analysing the data obtained by the authors [99, 121–141], a graph of minimization of internal stresses depending on temperature and holding time was constructed (Fig. 15). It should be noted that the graph presented in Fig. 15 is only a surface analysis, since the authors of the works [99, 121–141] used various methods to determine internal stresses, for example, x-ray diffraction (XRD), neutron diffraction (ND), *etc*. Various laboratory furnaces with different oxidation protection systems and cooling methods were used, for example, vacuum, protective medium — argon or nitrogen, *etc*.

As a result of the analytical studies and the establishment of the dependence based on literature data, it can be said that the influence of heat treatment conditions, holding time and cooling rate on the microstructure, mechanical and operational properties of 316L steel has been studied many times and by a large number of researchers in the temperature range of 388–1200 °C [142–151]. However, it should be noted that these studies did not pay enough attention to the influence of internal stresses.

Nevertheless, the studies of microstructure and mechanical properties reported in Refs. [142–151] established that, above 600 °C, chromium carbides form at grain boundaries, reducing corrosion resistance. Thus, increasing the temperature during heat treatment to relieve internal stresses has negative consequences.

To relieve significantly internal stresses, the heat treatment temperature should be above 900 °C, as suggested in the standard [71]. However, the characteristic grain structure in 316L is lost above 800 °C [137, 150, 151], and properties such as tensile strength [48, 152] and tensile strength [153] are reduced. The grain structure in 316L effectively hinders dislocation movement and thus does not increase tensile strength. On the other hand, low-temperature heat treatment (470 °C for 5 hours) did not improve tensile strength [154]. Based on the results above, the authors of

Refs. [136, 151] established that heat treatment at 600 °C for 4 hours is effective for relaxing internal stresses, while preserving the grain structure. Thus, conducting studies of the influence of heat treatment on the minimisation of residual stresses, the evolution of the microstructure, and mechanical properties is definitely relevant.

## 4. Conclusions

The systematisation of experimental and theoretical studies on the peculiarities of the formation of residual internal stresses in AISI 316L steel products manufactured using the LPBF technology has allowed us to generalise the key factors determining the stress-strain state of such materials and to assess the effectiveness of the main approaches to regulating it. The generalisations obtained can serve as the basis for scientifically substantiated recommendations to optimise the LPBF-process parameters and select rational post-processing modes to increase the structural stability and operational reliability of additively manufactured parts.

(i) It is generalised that the formation of residual internal stresses in parts made of AISI 316L steel manufactured by the LPBF technology is a consequence of the combination of ultra-high cooling rates, significant temperature gradients, and complex geometry of the products. The greatest contribution to the stress-strain state is made by the parameters of laser scanning, the strategy of layer construction, the density of applied energy, and the conditions of heat removal, which leads to the predominance of tensile stresses on the surface and compressive stresses in the volume of the product.

(ii) It is shown that the optimisation of the technological parameters of the LPBF process and scanning strategies (changing the orientation and size of the fields, rotation of the layers, multiple scanning, *etc.*) allows for partially reducing the level of residual stresses and deformations, but does not ensure their complete minimisation, especially for products with complex geometry and variable cross-section.

(iii) Generalisation of world experience shows that heat treatment to relieve internal stresses is the most effective and technologically justified method of stabilising the stressed state of the LPBF products made of AISI 316L steel. Rational selection of temperature, holding time, and environment allows achieving a significant reduction in residual stresses without deterioration of mechanical properties, which determines the prospects of a combined approach, namely, optimisation of printing parameters in combination with post-processing, for the practical implementation of the technology.

**Acknowledgment.** The authors express their gratitude to Olena Adolfivna Shpak and Lyudmyla Ivanivna Shvets for their assistance in preparing samples for microstructure analysis.

REFERENCES

1. S. Adjamskiy, G. Kononenko, R. Podolskyi, and S. Badyuk, *Implementation of Selective Laser Melting Technology in Ukraine* (Kyiv: Naukova Dumka: 2022) (in Ukrainian);
https://doi.org/10.15407/978-966-00-1856-3
2. D. Fu, X. Li, M. Zhang, M. Wang, Z. Zhang, and S. Qu, Influence of effective laser energy on the structure and mechanical properties of laser melting deposited Ti–6Al–4V alloy. *Materials*, **13**, No. 4: 962 (2020);
https://doi.org/10.3390/ma13040962
3. H. Gong, H. Gu, K. Zeng, J.J.S. Dilip, D. Pal, and B. Stucker, Melt pool characterization for selective laser melting of Ti–6Al–4V pre-alloyed powder, *Int. Solid Freeform Fabrication Symposium* (Austin: The University of Texas at Austin: 2014), p. 256–267;
https://doi.org/10.26153/tsw/15682
4. J.J.S. Dilip, M.A. Anam, D. Pal, and B. Stucker, A short study on the fabrication of single track deposits in SLM and characterization, *Proc. 26th Annual Int. Solid Freeform Fabrication Symposium (2016)*, p. 1644–1659.
5. C. Teng, H. Gong, A. Szabo, J.J.S. Dilip, K. Ashby, S. Zhang, N. Patil, D. Pal, and B. Stucker, Simulating melt pool shape and lack of fusion porosity for selective laser melting of cobalt–chromium components, *J. Manuf. Sci. Eng.*, **139**: 011009 (2017);
https://doi.org/10.1115/1.4034137
6. J.-H. Wang, J. Ren, W. Liu, X.-Y. Wu, M.-X. Gao, and P.-K. Bai, Effect of selective laser melting process parameters on microstructure and properties of Co–Cr alloy, *Materials*, **11**: 1546 (2018);
https://doi.org/10.3390/ma11091546
7. S.V. Adzhamskyi, G.A. Kononenko, and R.V. Podolskyi, Justification of technological modes for the formation of a stable single track at a thickness of a 30-μm layer of INCONEL 718 alloy, *System Technologies*, **2**, No. 145: 43–52 (2023) (in Ukrainian);
https://doi.org/10.34185/1562-9945-2-145-2023-05
8. Y. Guo, L. Jia, B. Kong, N. Wang, and H. Zhang, Single track and single layer formation in selective laser melting of niobium solid solution alloy, *Chinese J. Aeronautics*, **31**, No. 4: 860–866 (2018).
9. Z. Hu, B. Nagarajan, X. Song, R. Huang, W. Zhai, and J. Wei, Formation of SS316L single tracks in micro selective laser melting: surface, geometry, and defects, *Adv. Mater. Sci. Eng.*, **2019**: 9451406-1–9 (2019);
https://doi.org/10.1155/2019/9451406
10. S.V. Chernyshikhin, D.G. Firsov, and I.V. Shishkovsky, Selective laser melting of pre-alloyed NiTi powder: single-track study and FE modeling with heat source calibration, *Materials*, **14**: 7486 (2021);
https://doi.org/10.3390/ma14237486
11. J. Katagiri, M. Kusano, S. Minamoto, H. Kitano, K. Daimaru, M. Tsujii, and M. Watanabe, Melt pool shape evaluation by single-track experiments and finite-element thermal analysis: balling and lack-of-fusion criteria for generating process window of Inconel 738LC, *Materials*, **16**: 1729 (2023);
https://doi.org/10.3390/ma16041729
12. A. Antikainen, J. Reijonen, J. Lagerbom, M. Lindroos, T. Pinomaa, and T. Lindroos, Single-track laser scanning as a method for evaluating printability: The effect of substrate heat treatment on melt pool geometry and cracking in medium carbon tool steel, *J. Mater. Eng. Perform.*, **31**: 8418–8432 (2022);
https://doi.org/10.1007/s11665-022-06826-0

13. A. Mauduit, H. Gransac, P. Auguste, and S. Pillot, Study of AlSi7Mg0.6 alloy by selective laser melting: Mechanical properties, microstructure, heat treatment. *J. Casting Mater. Eng.*, **3**, No. 1: 1–13 (2019); https://doi.org/10.7494/jcme.2019.3.1.1
14. M. Letenneur, A. Kreitcberg, and V. Brailovski, Optimization of laser powder bed fusion processing using a combination of melt pool modeling and design of experiment approaches: Density control, *J. Manuf. Mater. Process.*, **3**: 21 (2019); https://doi.org/10.3390/jmmp3010021
15. S. Wang, L. Wang, J. Liu, R. Yang, J. Li, and G. Wang, Effects of laser energy density on morphology features and microstructures of the single molten track in selective laser melting, *Front. Mater.*, **10**: 1110844 (2023); https://doi.org/10.3389/fmats.2023.1110844
16. W. Wang and X. Liu, Effect of linear energy density on pores of 316L stainless steel by selective laser melting, *IOP Conf. Ser.: Earth Environ. Sci.*, **233**: 032008 (2019); https://doi.org/10.1088/1755-1315/233/3/032008
17. Y. Shi, C. Yan, Y. Zhou, J. Wu, Y. Wang, S. Yu, and Y. Chen, Metal materials for additive manufacturing, *Materials for Additive Manufacturing* (Academic Press: 2021), Ch. 5, p. 403–595; https://doi.org/10.1016/B978-0-12-819302-0.00005-5
18. Q. Deng, X. Wang, Q. Lan, N. Su, Y. Wu, and L. Peng, Limitations of linear energy density for laser powder bed fusion of Mg–15Gd–1Zn–0.4Zr Alloy, *SSRN*: 1–19 (2021); https://doi.org/10.2139/ssrn.3978442
19. S.V. Adzhams'kyy and H.A. Kononenko, Study of technological parameter influence on quality of Inconel 718 samples manufactured by SLM, *Metallofiz. Noveishie Tekhnol.*, **43**, No. 6: 741–752 (2021); https://doi.org/10.15407/mfint.43.06.0741
20. S. Adjamskiy, G. Kononenko, R. Podolskyi, and S. Baduk, Studying the influence of orientation and layer thickness on the physico-mechanical properties of Co–Cr–Mo alloy manufactured by the SLM method, *Sci. Innovation*, **18**, No. 5: 85–94 (2022); https://doi.org/10.15407/scine18.05.085
21. S.V. Adzhamskyy, H.A. Kononenko, and R.V. Podolskyi, Analysis of structure after heat treatment of Inconel 718 made by SLM, *Metallofiz. Noveishie Tekhnol.*, **43**, No. 7: 909–924 (2021); https://doi.org/10.15407/mfint.43.07.0909
22. J.-P. Kruth, M.-C. Leu, and T. Nakagawa, Progress in additive manufacturing and rapid prototyping, *CIRP Annals — Manuf. Technol.*, **47**, No. 2: 525–540 (1998); https://doi.org/10.1016/S0007-8506(07)63240-5
23. M.J. Donachie and S.J. Donachie, *Superalloys: A Technical Guide* (ASM International: 2002); https://doi.org/10.31399/asm.tb.stg2.9781627082679
24. D. Deng, *Additively Manufactured Inconel 718: Microstructures and Mechanical Properties* (Linköping University: 2018); https://doi.org/10.3384/lic.diva-144491
25. F. Hanning, *Weld Cracking in Precipitation–Hardening Ni-Based Superalloys* (Chalmers University of Technology: 2018).
26. C.T. Sims, N.S. Stoloff, and W.C. Hagel, *Superalloys II: High-Temperature Materials for Aerospace and Industrial Power* (Wiley: 1987).
27. G. Sjoberg and N.-G. Ingesten, Grain boundary δ-phase morphologies, carbides and notch rupture sensitivity of cast alloy 718, *TMS*: 603–620 (1991).

28. J. Andersson, *Weldability of Precipitation Hardening Superalloys–Influence of Microstructure. Department of Materials and Manufacturing Technology* (Chalmers University of Technology: 2011).
29. A. Mitchell, The precipitation of primary carbides in alloy 718, *Superalloys 718, 625, 706 and Derivatives* (Ed. E.A. Loria) (TMS: 2005), p. 65–78.
30. J.J. Schirra, The effect of Laves phase on the mechanical properties of wrought and cast + HIP Inconel 718 *Superalloys 718, 625, 706 and Derivatives* (Ed. E.A. Loria) (TMS: 1991), p. 375–388.
31. T. Kurzynowski, K. Gruber, W. Stopyra, B. Kuźnicka, and E. Chlebus, Correlation between process parameters, microstructure and properties of 316L stainless steel processed by selective laser melting, *Mater. Sci. Eng. A*, **718**: 64–73 (2018); https://doi.org/10.1016/j.msea.2018.01.103
32. L. Hitzler, J. Hirsch, B. Heine, M. Merkel, W. Hall, and A. Ochsner, On the anisotropic mechanical properties of selective laser-melted stainless steel, *Materials*, **10**: 1136 (2017);
https://doi.org/10.3390/ma10101136
33. M. Garibaldi, I. Ashcroft, M. Simonelli, and R. Hague, Metallurgy of high-silicon steel parts produced using selective laser melting, *Acta Mater.*, **110**: 207–216 (2016); https://doi.org/10.1016/j.actamat.2016.03.037
34. M.S.I.N. Kamariah, W.S.W. Harun, N.Z. Khalil, F. Ahmad, M.H. Ismail, and S. Sharif, Effect of heat treatment on mechanical properties and microstructure of selective laser melting 316L stainless steel, *IOP Conf. Ser.: Mater. Sci. Eng.*, **257**: 012021 (2017);
https://doi.org/10.1088/1757-899X/257/1/012021
35. C. Valero-Vidal, L. Casabán-Julián, I. Herraiz-Cardona, and A. Igual-Mucoz, Influence of carbides and microstructure of CoCrMo alloys on their metallic dissolution resistance. *Mater. Sci. Eng. C*, **33**, No. 8: 4667–4676 (2013);
https://doi.org/10.1016/j.msec.2013.07.041
36. K. Yamanaka, M. Mori, and A. Chiba, Assessment of precipitation behavior in dental castings of a Co–Cr–Mo alloy, *J. Mech. Behav. Biomed. Mater.*, **50**: 268–276 (2015); https://doi.org/10.1016/j.jmbbm.2015.06.020
37. P. Tunthawiroon, Y. Li, Y. Koizumi, and A. Chiba, Strain-controlled iso-thermal fatigue behavior of Co–29Cr–6Mo used for tooling materials in Al die casting. *Mater. Sci. Eng. A*, **703**: 27–36 (2017);
https://doi.org/10.1016/j.msea.2017.07.047
38. S.G. Ghalme, A. Mankar, and Y. Bhalerao, Biomaterials in hip joint replacement. *Int. J. Mater. Sci. Eng.*, **4**: 113–125 (2016).
39. K. Vutova, V. Stefanova, M. Markov, and V. Vassileva, Study on hardness of heat-treated cocrmo alloy recycled by electron beam melting, *Materials*, **16**, No. 7: 2634 (2023);
https://doi.org/10.3390/ma16072634
40. O. Babachenko, T. Balakhanova, O. Safronova, and R. Podolskyi, Specific features of the formation of structural heterogeneity in carbon steel depending on manufacturing technique, *Sci. Innovation*, **19**, No. 4: 47–56 (2023);
https://doi.org/10.15407/scine19.04.047
41. J.V. Giacchi, O. Fornaro, and H. Palacio, Microstructural evolution during solution treatment of CoCr–Mo–C biocompatible alloys, *Mater. Charact.*, **68**: 49–57 (2012); https://doi.org/10.1016/j.matchar.2012.03.006
42. P. Tunthawiroon and A. Chiba, Characterization of intermetallic phase in as-cast Si-doped Co–Cr–Mo alloys. *IOP Conf. Ser.: Mater. Sci. Eng.*, **635**: 012007 (2019); https://doi.org/10.1088/1757-899X/635/1/012007

43. W. Chen, T. Voisin, Y. Zhang, J.-B. Forien, C.M. Spadaccini, D.L. McDowell, T. Zhu, and Y.M. Wang, Microscale residual stresses in additively manufactured stainless steel, *Nat. Commun.*, **10**: 4338 (2019);
https://doi.org/10.1038/s41467-019-12265-8
44. W.E. Frazier, Metal additive manufacturing: A review, *J. Mater. Eng. Perform.*, **23**: 1917–1928 (2014);
https://doi.org/10.1007/s11665-014-0958-z
45. J.H. Martin, B.D. Yahata, J.M. Hundley, J.A. Mayer, T.A. Schaedler, and T.M. Pollock, 3D printing of high-strength aluminium alloys, *Nature*, **549**: 365–369 (2017);
https://doi.org/10.1038/nature23894
46. D. Herzog, V. Seyda, E. Wycisk, and C. Emmelmann, Additive manufacturing of metals, *Acta Mater.*, **117**: 371–392 (2016);
https://doi.org/10.1016/j.actamat.2016.07.019
47. T. DebRoy, H.L. Wei, J.S. Zuback, T. Mukherjee, J.W. Elmer, J.O. Milewski, A.M. Beese, A. Wilson-Heid, A. De, and W. Zhang, Additive manufacturing of metallic components — Process, structure and properties, *Prog. Mater. Sci.*, **92**: 112–224 (2017);
https://doi.org/10.1016/j.pmatsci.2017.10.001
48. Y.M. Wang, T. Voisin, J.T. McKeown, J. Ye, N.P. Calta, Z. Li, Z. Zeng, Y. Zhang, W. Chen, T.T. Roehling, R.T. Ott, M.K. Santala, P.J. Depond, M.J. Matthews, A.V. Hamza, and T. Zhu, Additively manufactured hierarchical stainless steels with high strength and ductility, *Nat. Mater.*, **17**: 63–71 (2018);
https://doi.org/10.1038/nmat5021
49. S.V. Adzhamskyi, G.A. Kononenko, and R.V. Podolskyi, Influence of SLM process parameters on the formation of the boundary region of parts made of heat-resistant nickel alloy Inconel 718, *Space Sci. Technol.*, **27**, 6: 105–114 (2021) (in Ukrainian);
https://doi.org/10.15407/knit2021.06.105
50. N.J. van Eck and L. Waltman, V*OSviewer: Visualizing Scientific Landscapes* (Centre for Science and Technology Studies, Leiden University);
https://www.vosviewer.com
51. OpenAlex, OpenAlex: an open bibliometric database of scientific publications;
https://api.openalex.org
52. Gephi Consortium, Gephi (version 0.10.1), open-source software for network visualization and analysis;
https://gephi.org
53. R.V. Podolskyi, S.V. Adzhamskyy, G.A. Kononenko, and S.I. Badyuk, The Influence of Physical Phenomena and Material Properties on the Quality of Parts during Selective Laser Melting, *Prog. Phys. Met.*, **26**, No. 4: 796–827 (2025);
https://doi.org/10.15407/ufm.26.04.796
54. B. Vayre, F. Vignat, and F. Villeneuve, Metallic additive manufacturing: state-of-the-art review and prospects, *Mech. Ind.*, **13**: 89–96 (2012);
https://doi.org/10.1051/meca/2012003
55. D.D. Gu, W. Meiners, K. Wissenbach, and R. Poprawe, Laser additive manufacturing of metallic components: materials, processes and mechanisms, *Int. Mater. Rev.*, **57**, No. 3: 133–164 (2012);
https://doi.org/10.1179/1743280411Y.0000000014
56. K.V. Wong and A. Hernandez, A review of additive manufacturing, *ISRN Mechanical Engineering*, **2012**: 208760-1–10 (2012);
https://doi.org/10.5402/2012/208760
57. D. Brackett, I. Ashcroft, and R. Hague, Topology optimization for additive manufacturing, *Proc. Solid Freeform Fabrication Symp.* (Austin, Texas: 2011), p. 348–362.

58. E.V. Parusov, I.M. Chuiko, S.I. Gubenko, E.V. Oliinyk, and O.V. Parusov, Influence of temperature-deformation parameters of thermomechanical treatment on the structure and mechanical properties of low-carbon alloyed steel, *Mater. Sci.*, **61**: 42–49 (2025);
https://doi.org/10.1007/s11003-025-00960-5
59. E. Parusov, I. Chuiko, S. Bobyr, E. Oliinyk, and V. Zhukov, On the formation of martensite in low-carbon alloy steel wire rod for welding applications during slow continuous cooling, *Key Eng. Mater.*, **1041**: 3–9 (2026);
https://doi.org/10.4028/p-sW6lDI
60. S. Adjamskiy, G. Kononenko, and R. Podolskyi, Mechanical properties of heat-resistant superalloy Inconel 718 obtained by selective laser melting and heat treatment under different load directions, *Sci. J. Ternopil National Technical University*, **99**, No. 3: 75–85 (2020) (in Ukrainian);
https://doi.org/10.33108/visnyk_tntu2020.03.075
61. H.A. Kononenko, S.V. Adzhamskyy, R.V. Podolskyi, O.A. Safronova, and E.A. Shpak, Comparative studies of the mechanical properties of 316L steel samples manufactured on the ALFA-150 machine for compliance with world analogues, *Fundamental and Applied Problems of Ferrous Metallurgy*, **36**: 370–378 (2022) (in Ukrainian);
https://doi.org/10.52150/2522-9117-2022-36-370-378
62. S. Bobyr, E. Parusov, T. Golubenko, and I. Chuiko, Diffusion model of austenite decomposition with considering its stabilizationin in alloyed steel, *Metallofiz. Noveishie Tekhnol.*, **44**, No. 1: 31–45 (2022) (in Ukrainian);
https://doi.org/10.15407/mfint.44.01.0031
63. E.V. Parusov, I.M. Chuiko, E.V. Oliinyk, and O.V. Parusov, Recovery processes in hot-deformed austenite: the essence of phenomena, models, applications in industry, *Metallofiz. Noveishie Tekhnol.*, **47**, No. 9: 927–955 (2025) (in Ukrainian).
https://doi.org/10.15407/mfint.47.09.0927
64. S.V. Adzhamskiy, H.A. Kononenko, and R.V. Podolskyi, Manufacturing of an improved cooling system for a liquid rocket engine combustion chamber using additive technologies, *Aerospace Technique and Technology*, **3**: 42–48 (2021) (in Ukrainian);
https://doi.org/10.32620/aktt.2021.3.05
65. GOST 5632-2014, *Legirovannye Nerzhaveyushchie Stali i Splavy Korrozionno-Stoikie, Zharostoikie i Zharoprochnye* (Marki, Standartinform), 56 p.
66. EN 10253-3:2008, *Butt-Welding Pipe Fittings. Wrought Austenitic and Austenitic–Ferritic (Duplex) Stainless Steels without Specific Inspection Requirements*, 50 p.
67. DIN EN 10253-3:2009, *Rohrverbindungsstücke zum Stumpfschweißen. Austenitische und austenitisch–ferritische (Duplex) Knetstähle ohne besondere Prüfanforderungen*, 50 p.
68. JIS G 3214:2009, *Stainless Steel Forgings for Pressure Vessels*, 35 p.
69. AFNOR NFA EN 10216-5:2005, *Seamless Steel Tubes for Pressure Purposes. Technical Delivery Conditions. Part 5: Stainless Steel Tubes*, EDF R&D EDF Branche Energies, 45 p.
70. ASTM A312, *Standard Specifications for Seamless, Welded and Intensive Cold-Worked Austenitic Stainless Steel Pipes*, 47 p.
71. SAE AMS 2759/4B, *Aerospace Material Specification. Heat Treatment Austenitic Corrosion-Resistant Steel Parts*, 7 p.
72. D. Dye, H. Stone, and R. Reed, Intergranular and interphase microstresses, *Current Opinion in Solid State and Materials Science*, **5**: 31–37 (2001);
https://doi.org/10.1016/S1359-0286(00)00019-X

73. P.J. Withers and H.K.D.H. Bhadeshia, Residual stress. Part 1 — Measurement techniques, *Mater. Sci. Technol.*, **17**: 355–365 (2001); https://doi.org/10.1179/026708301101509980
74. V.S. Vakhrusheva, O.D. Malysh, and N.V. Hruzin, Determination of Residual Stresses in Pipes, *Phys. Metall. Heat Treat. Met.*, No. 1 (100): 8–13 (2023); ttps://doi.org/10.30838/J.PMHTM.2413.280323.8.939
75. J. Repper, P. Link, M. Hofmann, C. Krempaszky, W. Petry, and E. Werner, Interphase microstress measurements in IN 718 by cold neutron diffraction, *Appl. Phys. A*, **99**: 565–569 (2010); https://doi.org/10.1007/s00339-010-5607-2
76. B. Clausen, T. Lorentzen, and T. Leffers, Self-consistent modelling of the plastic deformation of FCC polycrystals and its implications for diffraction measurements of internal stresses, *Acta Mater.*, **46**: 3087–3098 (1998); https://doi.org/10.1016/S1359-6454(98)00014-7
77. F.J. Mo, G.G. Sun, J. Li, C.S. Zhang, H. Wang, Y. Chen, Z. Liu, Z.K. Yang, H.J. Li, Z.L. Yang, B. Pang, Y. Huang, Y. Tian, J. Gong, B. Chen, and S. Peng, Recent progress of residual stress distribution and structural evolution in materials and components by neutron diffraction measurement at RSND, *Quantum Beam Science*, **2**: 15 (2018); https://doi.org/10.3390/qubs2030015
78. P. Mercelis and J.-P. Kruth, Residual stresses in selective laser sintering and selective laser melting, *Rapid Prototyping J.*, **12**: 254–265 (2006); https://doi.org/10.1108/13552540610707013
79. A.E. Patterson, S.L. Messimer, and P.A. Farrington, Overhanging features and the SLM/DMLS residual stresses problem: Review and future research need, *Technologies*, **5**, No. 2: 15 (2017); https://doi.org/10.3390/technologies5020015
80. N. Nadammal, S. Cabeza, T. Mishurova, T. Thiede, A. Kromm, C. Seyfert, L. Farahbod, C. Haberland, J.A. Schneider, and P.D. Portella, Effect of hatch length on the development of microstructure, texture and residual stresses in selective laser melted superalloy Inconel 718, *Mater. Des.*, **134**: 139–150 (2017); https://doi.org/10.1016/j.matdes.2017.08.049
81. C.R. Knowles, T.H. Becker, and R.B. Tait, Residual stress measurements and structural integrity implications for selective laser melted Ti–6Al–4V, *South African J. Industrial Eng.*, **23**: 119–129 (2012); https://doi.org/10.7166/23-3-515
82. I. Serrano-Munoz, T. Fritsch, T. Mishurova, A. Trofimov, D. Apel, A. Ulbricht, A. Kromm, R. Hesse, A. Evans, and G. Bruno, On the interplay of microstructure and residual stress in LPBF IN718, *J. Mater. Sci.*, **56**: 5845–5867 (2021); https://doi.org/10.1007/s10853-020-05553-y
83. A.S. Wu, D.W. Brown, M. Kumar, G.F. Gallegos, and W.E. King, An experimental investigation into additive manufacturing-induced residual stresses in 316L stainless steel, *Metall. Mater. Trans. A*, **45**: 6260–6270 (2014); https://doi.org/10.1007/s11661-014-2549-x
84. S.D. Bagg, L.M. Sochalski-Kolbus, and J.R. Bunn, The effect of laser scan strategy on distortion and residual stresses of arches made with selective laser melting, *Proc. American Soc. Precision Eng.* (Raleigh, NC, USA: 2016), p. 1–5.
85. M. Schmidt, M. Merklein, D. Bourell, D. Dimitrov, T. Hausotte, K. Wegener, L. Overmeyer, F. Vollertsen, and G.N. Levy, Laser based additive manufacturing in industry and academia, *CIRP Annals — Manuf. Technol.*, **66**: 561–583 (2017); https://doi.org/10.1016/j.cirp.2017.05.011

86. T. Mishurova, S. Cabeza, K. Artzt, J. Haubrich, M. Klaus, C. Genzel, G. Requena, and G. Bruno, An assessment of subsurface residual stress analysis in SLM Ti–6Al–4V, *Materials*, **10**: 348 (2017);
https://doi.org/10.3390/ma10040348
87. S.V. Adzhamskiy, A.A. Kononenko, and R.V. Podolskyi, Investigation of the influence of SLM process modes on quality in the area of product contours, *Mater. Int. Sci. Tech. Conf. 'University Science–2020'* (Mariupol: 2020), p. 157–158 (in Russian).
88. R.J. Williams, A. Piglione, T. Rønneberg, C. Jones, M.-S. Pham, C.M. Davies, and P.A. Hooper, *In situ* thermography for laser powder bed fusion: Effects of layer temperature on porosity, microstructure and mechanical properties, *Additive Manufacturing*, **30**: 100880-1–14 (2019);
https://doi.org/10.1016/j.addma.2019.100880
89. B. Zheng, Y. Zhou, J.E. Smugeresky, J.M. Schoenung, and E.J. Lavernia, Thermal behavior and microstructure evolution during laser deposition with laser-engineered net shaping: Part II. Experimental investigation and discussion, *Metall. Mater. Trans. A*, **39**, No. 9: 2237–2245 (2008);
https://doi.org/10.1007/s11661-008-9566-6
90. S.V. Adzhamskiy and A.A. Kononenko, Patterns of influence of the parameters of the selective laser melting (SLM) process on the formation of a single layer of heat-resistant nickel alloy Inconel 718, *Beam Technologies in Welding and Material Processing*, **9**: 5–11 (2019) (in Russian).
91. A.K. Parida and K. Maity, Comparison the machinability of Inconel 718, Inconel 625 and Monel 400 in hot turning operation, *Eng. Sci. Technol. Int. J.*, **21**: 364–370 (2018);
https://doi.org/10.1016/j.jestch.2018.03.018
92. L.E. Criales, Y.M. Arısoy, B. Lane, S. Moylan, A. Donmez, and T. Özel, Laser powder bed fusion of nickel alloy 625: experimental investigations of effects of process parameters on melt pool size and shape with spatter analysis, *Int. J. Machine Tools Manuf.*, **121**: 22–36 (2017);
https://doi.org/10.1016/j.ijmachtools.2017.03.004
93. S.V. Adzhamskiy, A.A. Kononenko, and R.V. Podolskyi, Two-dimensional modeling of the non-stationary temperature field of a single track made of heat-resistant alloy INCONEL 718, *Mater. All-Ukrainian Sci. Methodological Conf. 'Problems of Mathematical Modeling'*, Vol. **1**, p. 42–45 (2020).
94. D. Wang, Study on energy input and its influences on single-track, multi-track, and multi-layer in SLM, *Int. J. Adv. Manuf. Technol.*, **58**: 1189–1199 (2012);
https://doi.org/10.1007/s00170-011-3443-y
95. J.J.S. Dilip, S. Zhang, and C. Teng, Influence of processing parameters on the evolution of melt pool, porosity, and microstructures in Ti-6Al-4V alloy parts fabricated by selective laser melting, *Prog. Additive Manuf.*, **2**: 157–167 (2017);
https://doi.org/10.1007/s40964-017-0030-2
96. A. Ulbricht, S.J. Altenburg, M. Sprengel, K. Sommer, G. Mohr, T. Fritsch, T. Mishurova, I. Serrano-Munoz, A. Evans, M. Hofmann, and G. Bruno, Separation of the Formation Mechanisms of Residual Stresses in LPBF 316L, *Metals*, **10**: 1234 (2020);
https://doi.org/10.3390/met10091234
97. J.L. Bartlett and X. Li, An overview of residual stresses in metal powder bed fusion, *Additive Manuf.*, **27**: 131–149 (2019);
https://doi.org/10.1016/j.addma.2019.02.020
98. M. Shiomi, K. Osakada, K. Nakamura, T. Yamashita, and F. Abe, Residual stress within metallic model made by selective laser melting process, *CIRP Annals —*

*Manuf. Technol.*, **53**, No.1: 195–198 (2004);
https://doi.org/10.1016/S0007-8506(07)60677-5
99. H. Nakamura, Y. Kawahito, K. Nishimoto, and S. Katayama, Elucidation of melt flows and spatter formation mechanisms during high power laser welding of pure titanium, *J. Laser Applications*, **27**, No. 3: 032012 (2015);
https://doi.org/10.2351/1.4922383
100. S.A. Khairallah, A.T. Anderson, A. Rubenchik, and W.E. King, Laser powder-bed fusion additive manufacturing: physics of complex melt flow and formation mechanisms of pores, spatter, and denudation zones, *Acta Mater.*, **108**: 36–45 (2016);
https://doi.org/10.1016/j.actamat.2016.02.014
101. R.J. Moat, A.J. Pinkerton, L. Li, P.J. Withers, and M. Preuss, Residual stresses in laser direct metal deposited Waspaloy, *Mater. Sci. Eng. A*, **528**: 2288–2298 (2011);
https://doi.org/10.1016/j.msea.2010.12.010
102. M. Grasso and B.M. Colosimo, Process defects and in situ monitoring methods in metal powder bed fusion: a review, *Measurement Sci. Technol.*, **28**: 1–25 (2017);
https://doi.org/10.1088/1361-6501/aa5c4f
103. Y. Lu, S. Wu, Y. Gan, T. Huang, C. Yang, J. Lin, and J. Lin, Study on the microstructure, mechanical property and residual stress of SLM Inconel-718 alloy manufactured by differing island scanning strategy, *Optics & Laser Technol.*, **75**: 197–206 (2015);
https://doi.org/10.1016/j.optlastec.2015.07.009
104. B. Dovgyy, A. Piglione, P. Hooper, and M.-S. Pham, Comprehensive assessment of the printability of CoNiCrFeMn in Laser Powder Bed Fusion, *Mater. Des.*, **194**: 108845 (2020);
https://doi.org/10.1016/j.matdes.2020.108845
105. R.V. Podolskyi, O.I. Babachenko, G.A. Kononenko, N.S. Romanova, A.O. Safronova, and E.S. Klemeshov, *Zastosuvannya Spetsializovanoho Prohramnoho Zabezpechennya v Materialoznavstvi ta Termichnii Obrobtsi Metaliv ta Splaviv: Metodychnyi Posibnyk* (Dnipro: UDUNT: 2022), 65 p. (in Ukrainian).
106. L.I. Muravskyi, *Metody Spekl-Koreliatsii dlya Doslidzhennya Mekhanichnykh Vlastyvostei Konstruktsiinykh Materialiv* (Kyiv: Naukova Dumka: 2010) (in Ukrainian).
107. I. Serrano-Munoz, A. Evans, T. Mishurova, M. Sprengel, T. Pirling, A. Kromm, and G. Bruno, The importance of subsurface residual stress in laser powder bed fusion IN718, *Adv. Eng. Mater.*, **24**, No. 6: 2100895 (2022);
https://doi.org/10.1002/adem.202100895
108. P. Pant, S. Proper, V. Luzin, S. Sjostrom, K. Simonsson, J. Moverare, S. Hosseini, V. Pacheco, and R.L. Peng, Mapping of residual stresses in as-built Inconel 718 fabricated by laser powder bed fusion: A neutron diffraction study of build orientation influence on residual stresses, *Additive Manufact.*, **36**: 101501 (2020);
https://doi.org/10.1016/j.addma.2020.101501
109. T. Thiede, S. Cabeza, T. Mishurova, N. Nadammal, A. Kromm, J. Bode, C. Haberland, and G. Bruno, Residual stress in selective laser melted Inconel 718: Influence of the removal from base plate and deposition hatch length, *Mater. Perform. Charact.*, **7**: 717–735 (2018);
https://doi.org/10.1520/MPC20170119
110. T. Mishurova, S. Cabeza, T. Thiede, N. Nadammal, A. Kromm, M. Klaus, C. Genzel, C. Haberland, and G. Bruno, The influence of the support structure on residual stress and distortion in SLM Inconel 718 parts, *Metall. Mater. Trans. A*, **49**: 3038–3046 (2018);
https://doi.org/10.1007/s11661-018-4653-9

111. C. Casavola, S.L. Campanelli, and C. Pappalettere, Preliminary investigation on distribution of residual stress generated by the selective laser melting process, *J. Strain Analysis Eng. Design*, **44**: 93–104 (2009);
https://doi.org/10.1243/03093247JSA464
112. J.-P. Kruth, J. Deckers, E. Yasa, and R. Wauthlé, Assessing and Comparing Influencing Factors of Residual Stresses in Selective Laser Melting Using a Novel Analysis Method, *Proc. Institution of Mechanical Engineers*, **226**: 980–991 (2012);
https://doi.org/10.1177/0954405412437085
113. L.N. Carter, C. Martin, P.J. Withers, and M.M. Attallah, The influence of the laser scan strategy on grain structure and cracking behavior in SLM powder-bed fabricated nickel superalloy, *J. Alloys Compd.*, **615**: 338–347 (2014);
https://doi.org/10.1016/j.jallcom.2014.06.172
114. K. Zhang, X. Zhang, and X. Shang, Research on cladding process of metal powder during laser additive manufacturing, *Appl. Mech. Mater.*, **380**: 4311–4314 (2013);
https://doi.org/10.4028/www.scientific.net/AMM.380-384.4311
115. F. Abe, K. Osakada, M. Shiomi, K. Uematsu, and M. Matsumoto, The manufacturing of hard tooling from metallic powders by selective laser melting, *J. Mater. Process. Technol.*, **111**: 210–213 (2001),
https://doi.org/10.1016/S0924-0136(01)00522-2
116. B. Qian, Y. Shi, Q. Wei, and H. Wang, The helix scan strategy applied to the selective laser melting, *Int. J. Adv. Manuf. Technol.*, **63**: 631–640 (2012);
https://doi.org/10.1007/s00170-012-3922-9
117. Y. Liu, Y. Yang, and D. Wang, A study on the residual stress during selective laser melting (SLM) of metallic powder, *Int. J. Adv. Manuf. Technol.*, **87**: 647–656 (2016);
https://doi.org/10.1007/s00170-016-8466-y
118. B. Cheng, S. Shrestha, and K.V. Chou, Stress and deformation evaluations of scanning strategy effect in selective laser melting, *Additive Manuf.*, **12**: 240–251 (2016);
https://doi.org/10.1016/j.addma.2016.05.007
119. M.M. Attallah, R. Jennings, X. Wang, and L.N. Carter, Additive manufacturing of Ni-based superalloys: The outstanding issues, *MRS Bulletin*, **41**: 758–764 (2016);
https://doi.org/10.1557/mrs.2016.211
120. M. Ghasri-Khouzani, H. Peng, R. Rogge, R. Attardo, P. Ostiguy, J. Neidig, R. Billo, D. Hoelzle, and M.R. Shankar, Experimental measurement of residual stress and distortion in additively manufactured stainless steel components with various dimensions, *Mater. Sci. Eng. A*, **707**: 689–700 (2017);
https://doi.org/10.1016/j.msea.2017.09.108
121. M.L. Montero Sistiaga, S. Nardone, C. Hautfenne, and J. Van Humbeeck, Effect of heat treatment of 316L stainless steel produced by selective laser melting (SLM), *Proc. 2016th Int. Solid Freeform Fabrication Symposium – An Additive Manufacturing Conf.* (University of Texas at Austin: 2016), p. 558–565.
122. J. Drapala, G. Kostiukova, and M. Losertova, Influence of heat treatment on microstructure and mechanical properties of SUS 316L alloy, *Proc. 27th Int. Conf. Metallurgy and Materials* (Ostrava, Czech Republic: Technical University of Ostrava: 2018), p. 1527–1532.
123. K. Chadha, Y. Tian, J.G. Spray, and C.Jr. Aranas, Effect of annealing heat treatment on the microstructural evolution and mechanical properties of hot isostatic

pressed 316L stainless steel, *Metals*, **10**: 753 (2020);
https://doi.org/10.3390/met10060753
124. I. Segura, L.E. Murr, C. Terrazas, D. Bermudez, J. Mireles, V. Injeti, K. Li, B. Yu, R.D.K. Misra, and R.B. Wicker, Grain boundary and microstructure engineering of Inconel 690 cladding on stainless-steel 316L using electron-beam powder bed fusion additive manufacturing, *J. Mater. Sci. Technol.*, **35**: 351–367 (2019);
https://doi.org/10.1016/j.jmst.2018.09.059
125. A. Röttger, K. Geenen, M. Windmann, F. Binner, and W. Theisen, Comparison of microstructure and mechanical properties of 316L austenitic steel processed by selective laser melting with hot-isostatic pressed and cast material, *Mater. Sci. Eng. A*, **678**: 365–376 (2016);
https://doi.org/10.1016/j.msea.2016.10.012
126. H.D. Carlton, A. Haboub, G.F. Gallegos, D.Y. Parkinson, and A.A. MacDowell, Damage evolution and failure mechanisms in additively manufactured stainless steel, *Mater. Sci. Eng. A*, **651**: 406–414 (2016);
https://doi.org/10.1016/j.msea.2015.10.073
127. S. Leuders, T. Lieneke, S. Lammers, T. Tröster, and T. Niendorf, On the fatigue properties of metals manufactured by selective laser melting — the role of ductility, *J. Mater. Res.*, **29**, No. 17: 1911–1919 (2014);
https://doi.org/10.1557/jmr.2014.157
128. T.M. Mower and M.J. Long, Mechanical behavior of additive manufactured, powder bed laser-fused materials, *Mater. Sci. Eng. A*, **651**: 198–213 (2016);
https://doi.org/10.1016/j.msea.2015.10.068
129. D. Kong, C. Dong, X. Ni, L. Zhang, J. Yao, C. Man, X. Cheng, K. Xiao, and X. Li, Mechanical properties and corrosion behavior of selective laser melted 316L stainless steel after different heat treatment processes, *J. Mater. Sci. Technol.*, **35**, No. 7: 1499–1507 (2019);
https://doi.org/10.1016/j.jmst.2019.03.003
130. D. Kong, X. Ni, C. Dong, L. Zhang, C. Man, J. Yao, K. Xiao, and X. Li, Heat treatment effect on the microstructure and corrosion behavior of 316L stainless steel fabricated by selective laser melting for proton exchange membrane fuel cells, *Electrochim. Acta*, **276**: 293–303 (2018);
https://doi.org/10.1016/j.electacta.2018.04.188
131. Q. Chao, S. Thomas, N. Birbilis, P. Cizek, P.D. Hodgson, and D. Fabijanic, The effect of post-processing heat treatment on the microstructure, residual stress and mechanical properties of selective laser melted 316L stainless steel, *Mater. Sci. Eng. A*, **821**: 141611 (2021);
https://doi.org/10.1016/j.msea.2021.141611
132. V. Cruz, Q. Chao, N. Birbilis, D. Fabijanic, P.D. Hodgson, and S. Thomas, Electrochemical studies on the effect of residual stress on the corrosion of 316L manufactured by selective laser melting, *Corrosion Sci.*, **164**: 108314 (2020);
https://doi.org/10.1016/j.corsci.2019.108314
133. S. Santa-Aho, M. Kiviluoma, T. Jokiaho, T. Gundgire, M. Honkanen, M. Lindgren, and M. Vippola, Additive manufactured 316L stainless-steel specimens: Microstructure, residual stress and corrosion characteristics after post-processing, *Metals*, **11**: 182 (2021);
https://doi.org/10.3390/met11020182
134. D. Riabov, A. Leicht, J. Ahlström, and E. Hryha, Investigation of the strengthening mechanism in 316L stainless steel produced with laser powder bed fusion, *Mater. Sci. Eng. A*, **822**: 141699 (2021);
https://doi.org/10.1016/j.msea.2021.141699

135. C. Yu, A. Leicht, V. Luzin, M. Busi, E. Polatidis, M. Strobl, R.L. Peng, and J.J. Moverare, Effect of Stress Relief Heat Treatment on Low Cycle Fatigue Behaviours of LPBF Stainless Steel 316L, *SSRN*;
https://doi.org/10.2139/ssrn.4159502
136. M. Gel'atko, M. Hatala, F. Botko, R. Vandžura, J. Hajnyš, M. Šajgalík, and J. Török, Stress relieving heat treatment of 316L stainless steel made by additive manufacturing process, *Materials*, **16**: 6461 (2023);
https://doi.org/10.3390/ma16196461
137. M. Sprengel, A. Ulbricht, A. Evans, A. Kromm, K. Sommer, T. Werner, J. Kelleher, G. Bruno, and T. Kannengiesser, Towards the optimization of post-laser powder bed fusion stress-relieve treatments of stainless steel 316L, *Metall. Mater. Trans. A*, **52**: 5342–5356 (2021);
https://doi.org/10.1007/s11661-021-06472-6
138. W.J. Lai, A. Ojha, Z. Li, C. Engler-Pinto, and X. Su, Effect of residual stress on fatigue strength of 316L stainless steel produced by laser powder bed fusion process, *Prog. Additive Manuf.*, **6**: 375–383 (2021);
https://doi.org/10.1007/s40964-021-00164-8
139. A. Riemer, S. Leuders, M. Thöne, H.A. Richard, T. Tröster, and T. Niendorf, On the fatigue crack growth behavior in 316L stainless steel manufactured by selective laser melting, *Eng. Fracture Mech.*, **120**: 15–25 (2014);
https://doi.org/10.1016/j.engfracmech.2014.03.008
140. R.J. Williams, F. Vecchiato, J. Kelleher, M.R. Wenman, P.A. Hooper, and C.M. Davies, Effects of heat treatment on residual stresses in the laser powder bed fusion of 316L stainless steel: Finite element predictions and neutron diffraction measurements, *J. Manuf. Proc.*, **57**: 641–653 (2020);
https://doi.org/10.1016/j.jmapro.2020.07.023
141. J. Douthett, *ASM Handbook* (ASM International: 1991), p. 1682–1708.
142. B. Al-Mangour, P. Vo, and R. Mongrain, Effect of heat treatment on the microstructure and mechanical properties of stainless steel 316L coatings produced by cold spray for biomedical applications, *J. Thermal Spray Technol.*, **23**: 641–652 (2014);
https://doi.org/10.1007/s11666-013-0053-2
143. M. Atapour, X. Wang, K. Färnlund, I.O. Wallinder, and Y. Hedberg, Corrosion and metal release investigations of selective laser melted 316L stainless steel in a synthetic physiological fluid containing proteins and in diluted hydrochloric acid, *Electrochim, Acta*, **354**: 136748 (2020);
https://doi.org/10.1016/j.electacta.2020.136748
144. O.O. Salman, C. Gammer, A.K. Chaubey, J. Eckert, and S. Scudino, Effect of heat treatment on microstructure and mechanical properties of 316L steel synthesized by selective laser melting, *Mater. Sci. Eng. A*, **748**: 205–212 (2019);
https://doi.org/10.1016/j.msea.2019.01.110
145. A.-H. Puichaud, C. Flament, A. Chniouel, F. Lomello, E. Rouesne, P.-F. Giroux, H. Maskrot, F. Schuster, and J.-L. Béchade, Microstructure and mechanical properties relationship of additively manufactured 316L stainless steel by selective laser melting, *EPJ Nuclear Sci. Technol.*, **5**: 23 (2019);
https://doi.org/10.1051/epjn/2019051
146. A.F. Padilha, R.L. Plaut, and P.R. Rios, *Stainless Steel Heat Treatment* (Boca Raton: CRC Press: 2006), p. 706–751.
147. M. Laleh, A.E. Hughes, W. Xu, P. Cizek, and M.Y. Tan, Unanticipated drastic decline in pitting corrosion resistance of additively manufactured 316L stainless

steel after high-temperature post-processing, *Corrosion Sci.*, **165**: 108412 (2019); https://doi.org/10.1016/j.corsci.2019.108412

148. N. Haghdadi, M. Laleh, M. Moyle, and S. Primig, Additive manufacturing of steels: a review of achievements and challenges, *J. Mater. Sci.*, **56**: 64–107 (2021);
https://doi.org/10.1007/s10853-020-05109-0
149. L. Wiesent, U. Schultheiß, P. Lulla, A. Nonn, and U. Noster, Mechanical properties of small structures built by selective laser melting 316L stainless steel — a phenomenological approach to improve component design, *Materialwiss. Werkstoff.*, **51**: 1615 (2020);
https://doi.org/10.1002/mawe.202000038
150. L. Cui, S. Jiang, J. Xu, R.L. Peng, R.T. Mousavian, and J. Moverare, Revealing relationships between microstructure and hardening nature of additively manufactured 316L stainless steel, *Mater. Des.*, **198**: 109385 (2021);
https://doi.org/10.1016/j.matdes.2020.109385
151. J.D. Fritz, *Heat Treating of Austenitic and Duplex Stainless Steels* (ASM International: 2018);
https://doi.org/10.31399/asm.hb.v04d.a0005990
152. L. Liu, Q. Ding, Y. Zhong, J. Zou, J. Wu, Y.-L. Chiu, J. Li, Z. Zhang, Q. Yu, and Z. Shen, Dislocation network in additive manufactured steel breaks strength–ductility trade-off, *Mater. Today*, **21**, No. 4: 354–361 (2018);
https://doi.org/10.1016/j.mattod.2017.11.004
153. L. Cui, F. Jiang, D. Deng, T. Xin, X. Sun, R.T. Mousavian, R.L. Peng, Z. Yang, and J. Moverare, Cyclic response of additive manufactured 316L stainless steel: The role of cell structures, *Scr. Mater.*, **205**: 114190 (2021);
https://doi.org/10.1016/j.scriptamat.2021.114190
154. C. Elangeswaran, A. Cutolo, G.K. Muralidharan, C. Formanoir, F. Berto, K. Vanmeensel, and B. Hooreweder, Effect of post-treatments on the fatigue behaviour of 316L stainless steel manufactured by laser powder bed fusion, *Int. J. Fatigue*, **123**: 31–39 (2019);
https://doi.org/10.1016/j.ijfatigue.2019.01.013

Received / Final version
25.02.2026 / 28.07.2026

*Г.А. Кононенко*[1,2,3], *П. Рамасамі*[4,5], *С.В. Аджамський*[1,6],
*Ю. Еккерт*[4,5], *Р.В. Подольський*[1,2,7], *О.А. Подольська*[2], *С.І. Бадюк*[1,7]
[1] ТОВ «Адитивні лазерні технології України»,
просп. Небесної Сотні, 105, 65104 Одеса, Україна
[2] Інститут чорної металургії ім. З.І. Некрасова НАН України,
пл. Академіка Стародубова, 1, 49107 Дніпро, Україна
[3] Національний технічний університет України
«Дніпровська політехніка»,
просп. Дмитра Яворницького, 19, 49005 Дніпро, Україна
[4] Інститут матеріалознавства Еріха Шміда Австрійської академії наук,
Янштрассе, 12, 8700 Леобен, Австрія
[5] Університет Монтана в Леобені,
Розеґґерштрассе, 12, 8700 Леобен, Австрія
[6] Інститут транспортних систем і технологій НАН України,
вул. Пісаржевського, 5, 49000 Дніпро, Україна
[7] Інститут прикладних систем управління НАН України,
просп. Академіка Глушкова, 40, 03187 Київ, Україна

## УТВОРЕННЯ ТА ЗМЕНШЕННЯ ЗАЛИШКОВИХ НАПРУЖЕНЬ У НЕРЖАВНІЙ СТАЛІ AISI 316L, ВИГОТОВЛЕНІЙ МЕТОДОМ ТОПЛЕННЯ В ПОРОШКОВОМУ ШАРІ ЗА ДОПОМОГОЮ ПОТУЖНОГО ЛАЗЕРНОГО ОПРОМІНЕННЯ: ОГЛЯД СТРАТЕГІЙ ОБРОБЛЯННЯ ТА ПІДХОДІВ ЩОДО ТЕРМІЧНОГО ОБРОБЛЕННЯ

Адитивне виробництво металевих виробів за технологією лазерного (селективного) топлення у порошковому шарі (LPBF) відкриває широкі можливості для виготовлення деталей складної геометрії зі сталей і сплавів. Водночас характерні для LPBF-технології високі температурні градієнти та надвисокі швидкості охолодження призводять до інтенсивного формування залишкових внутрішніх напружень, які неґативно впливають на геометричну стабільність, механічні властивості й експлуатаційну надійність виробів. У роботі виконано комплексний огляд сучасних національних і міжнародних досліджень, що стосуються механізмів формування та шляхів мінімізації залишкових напружень у деталях зі сталі AISI 316L, виготовлених за LPBF-технологією. З використанням мережевого бібліографічного аналізу (VOSviewer) з базою даних OpenAlex і кластеризацією за укладанням (Gephi) систематизовано ключові наукові напрями, параметри процесу та стратегії сканування, що мають визначальний вплив на напружено-деформований стан виробів. Проаналізовано роль геометрії деталей, товщини шару, густини лазерної енергії, орієнтації та розміру полів сканування у формуванні макро- та мікронапружень. Особливу увагу приділено аналізу нормативно-технічної документації та режимів термічного оброблення сталі AISI 316L та її аналогів, а також узагальненню світового досвіду застосування термічних методів зняття внутрішніх напружень для LPBF-виробів. Показано, що термічне оброблення є найефективнішим інструментом досягнення сприятливого рівня та розподілу залишкових напружень за умови збереження необхідного комплексу механічних властивостей. Одержані результати можуть бути використані для обґрунтування раціональних параметрів LPBF-процесу та постоброблення деталей зі сталі AISI 316L для критично важливих інженерних застосувань.

**Ключові слова:** сталь 316L, лазерне стоплення у порошковому шарі, залишкові напруження, термічне оброблення, технологічні параметри.